

Station-orientation catalog for Australian broadband seismic stations

K. Tarumi^{1,*} and K. Yoshizawa^{1,2}

¹ Department of Natural History Sciences, Graduate School of Science, Hokkaido University, Sapporo 060-0810, Japan

²Department of Earth & Planetary Sciences, Faculty of Science, Hokkaido University, Sapporo 060-0810, Japan.

*Corresponding author: tarumi.kotaro.jp@gmail.com

This is a preprint that is submitted to EarthArXiv. The original manuscript has been submitted to Pure and Applied Geophysics.

Station-orientation catalog for Australian broadband seismic stations

Kotaro Tarumi^{1*} and Kazunori Yoshizawa^{1,2†}

^{1*}Department of Natural History Sciences, Graduate School of Science, Hokkaido University, Sapporo, 0600810, Japan.

²Department of Earth and Planetary Sciences, Faculty of Science,
Hokkaido University, Sapporo, 0600810, Japan.

*Corresponding author(s). E-mail(s): tarumi.kotaro.jp@gmail.com;

Contributing authors: yoshizawa@sci.hokudai.ac.jp;

[†]These authors contributed equally to this work.

Abstract

Many broadband seismic stations deployed permanently and temporarily in the Australian continent have been used for various seismological investigations in and around Australia. Although two horizontal components are generally assumed to be oriented in the north and east directions, as reported by data providers, misorientations of horizontal components from the true geographic north direction cannot be avoided in practical field observations, even in the well-maintained permanent stations. In this paper, we applied a polarization analysis to almost all stations in Australia to estimate the misorientations of horizontal components using long-period teleseismic P-waves. A large data set of P-wave arrival angles allows us to successfully detect probable horizontal misorientations, including significant temporal changes in some stations, which generally happened at reported timings of station maintenance and instrument replacements. However, some stations exhibit misorientations and temporal changes at unexpected timings that are unreported, crucially affecting the earth's internal exploration, which could be evident from the teleseismic receiver function analyses, especially in the transverse component. Compiling the information on such time-dependent misorientations, we created a full catalog of horizontal-component orientations for both permanent and temporary stations in Australia, which are widely available for the community.

33

1 Introduction

34 A large number of broadband seismic stations deployed permanently or temporarily in
35 the Australian continent have provided key information on seismic wave propagation
36 (e.g., [Kennett and Furumura, 2008](#)), seismic sources (e.g., [Hejrani and Tkalcic, 2020](#)),
37 and seismic structure (e.g., [Kennett et al., 2013](#); [Yoshizawa, 2014](#); [Birkey and Ford,](#)
38 [2023](#); [Eakin et al., 2023](#)) in and around Australia. As an initial step for the three-
39 component seismic waveform analysis, we generally rotate two horizontal components
40 (e.g., NS / EW) to radial and transverse directions, supposing that the horizontal sen-
41 sors are oriented in the north and east (or in reported) directions. However, as several
42 earlier studies suggested, there is a possibility of nontrivial misorientation of horizontal
43 components at some stations (e.g., [Laske, 1995](#); [Yoshizawa et al., 1999](#); [Schulte-Pelkum](#)
44 et al., [2001](#)). Also, temporal changes in the amplitude gain of seismometers may occur
45 at some permanent stations over a long observation period ([Ekström et al., 2006](#)).
46 Such errors or uncertainties in the reported catalog values, particularly the ambigui-
47 ties in the horizontal-component orientation, would prevent us from performing precise
48 waveform analyses that depend on the horizontal directions, such as shear-wave split-
49 ting measurements, Love-wave dispersion analysis, and the azimuthal dependency of
50 receiver functions.

51 The horizontal orientation of seismic stations can be estimated by measuring the
52 arrival angles of teleseismic P or Rayleigh waves at longer periods for a large number of
53 seismic events (e.g., [Laske and Masters, 1996](#); [Yoshizawa et al., 1999](#); [Schulte-Pelkum](#)
54 et al., [2001](#); [Larson and Ekström, 2002](#); [Ekström and Busby, 2008](#)). Rayleigh waves
55 generally oscillate elliptically in the radial-vertical plane, but their particle motions

56 become more complicated in heterogeneous and anisotropic media (Crampin, 1975).
57 Moreover, due to the dispersive nature of surface waves, the arrival-angle anomalies
58 (or deviations from the great-circle path) depend significantly on the frequency (Laske,
59 Yoshizawa et al., 1999), which may increase uncertainties in the estimated sta-
60 tion orientation. Furthermore, the overlaps by preceding Love waves in the transverse
61 component make it difficult to perform arrival-angle analysis of Rayleigh waves at rel-
62 atively shorter epicentral distances of less than 50° (Yoshizawa et al., 1999). On the
63 contrary, the onset of teleseismic P-waves exhibits a relatively simple linear motion
64 in the radial-vertical plane without frequency dependence. Teleseismic P waves with
65 the near-vertical incidence to the station mainly sample the lower mantle where lat-
66 eral heterogeneities are weak. Thus, the ray-bending effects on P-waves due to strong
67 lateral heterogeneity in the upper mantle can be milder than that on surface waves
68 (Yoshizawa et al., 1999), in addition to the relatively smaller influence from anisotropy
69 on P-waves compared to surface waves (Crampin et al., 1982).

70 Recently, major seismological data centers, such as IRIS (Incorporated Research
71 Institutions for Seismology), have provided us with more precise information on the
72 station orientation for their affiliated stations worldwide, including Australian stations.
73 Given proper information from careful calibrations, many of the broadband horizontal
74 channels in major stations in global networks (such as the Global Seismograph Net-
75 work) have been named BH1 and BH2 (for the first and second components) rather
76 than conventional BHN and BHE (North and East), when the true horizontal direc-
77 tions deviate from the geographic north and east (Ekström and Busby, 2008). Ekström
78 (2008) has also provided practically useful tables on the station orientation for GSN
79 stations until 2015. However, a number of seismic stations from local data providers
80 and temporary seismic networks, including transportable seismic arrays (e.g., SKIPPY
81 in Australia; Hilst et al., 1994), still lack precise information on horizontal orienta-
82 tions, which is crucial for researchers wishing to utilize these valuable waveform data
83 sets.

84 In this paper, we collect a large number of P-wave arrival angle data to estimate the
 85 horizontal orientation of many broadband seismic stations in Australia, modeled on the
 86 method of polarization analysis by Vidale (1986) utilized in earlier study by Yoshizawa
 87 et al. (1999). Through the polarization analysis of teleseismic P-wave particle motions,
 88 we construct a complete catalog of the horizontal orientation of currently available
 89 broadband stations in Australia, which can be used for a variety of future applications
 90 of seismic data analyses with horizontal components.

91 2 Data and Method

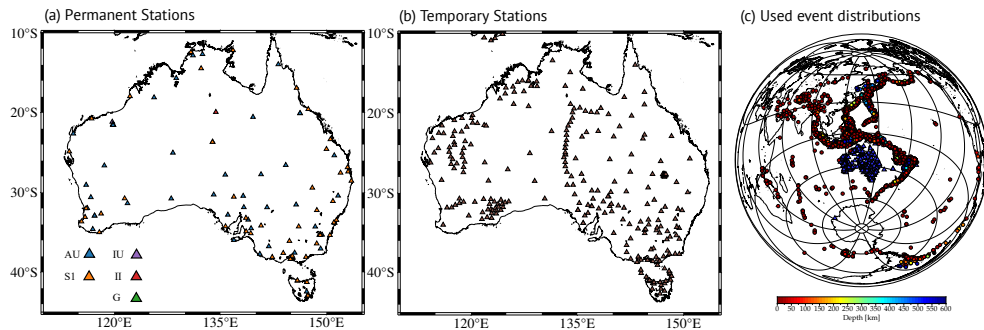


Fig. 1 Broadband seismic stations and seismic events used in this study. (a) Permanent stations, with colors indicating different networks (AU, S1, IU, II, and G). (b) Temporary stations. (c) Seismic events used in this study, with colors representing source depths. Blue triangles are employed stations in (a) and (b).

92 We used the three-component teleseismic P-wave data downloaded from the IRIS
 93 Data Management Center (IRIS DMC) and Australian Passive Seismic Server (Aus-
 94 Pass) for 4004 seismic events with moment magnitude $M_w \geq 5.5$ from 1987 to 2019.
 95 Our dataset includes both permanent and temporary broadband stations shown in
 96 Figures 1 (a, b). Permanent seismic networks include IRIS/IDA (red triangles in
 97 Figure 1 (a); Network II), IRIS/USGS (purple triangles in Figure 1 (a); Network IU),
 98 GEOSCOPE (green triangles in Figure 1 (a); Network G), GeoScience Australia (blue

99 triangles in Figure 1 (a); Network AU), and Australian Seismometers in Schools pro-
100 gram (orange triangles in Figure 1 (a); Network S1). Temporary stations shown in
101 Figure 1 (b) involve many temporary seismic arrays, SKIPPY ([Hilst and Kennett,](#)
102 [1993](#)), KIMBA ([Kennett, 1997, 1998](#)), QUOLL ([Kennett et al., 1999](#)), West Australia
103 Cratons [Kennet \(2000\)](#), TRIGGER BB ([Rawlinson and Kennett, 2001](#)), TASMAL
104 ([Kennett, 2003](#)), CARPA - Linkage ([Reading and Kennett, 2005](#)), SOC - Southern Cra-
105 ton ([Fontaine and Kennet, 2007](#)), BILBY ([Rawlinson and Kennet, 2008](#)), Bass Strait
106 ([Reading and Rawlinson, 2011](#)), Australia ([Tkalčić et al., 2013](#)), Albany-Fraser Experi-
107 ment ([Tkalčić et al., 2013](#)), and Transitions in the Banda Arc-Australia continental
108 collision ([Miller, 2014](#)).

109 We selected seismic events with $Mw \geq 5.5$, distance ranges between 30 and 90
110 degrees, and normalized amplitude of P-wave radiation $> |0.3|$ estimated from the
111 Global CMT catalog ([Dziewonski et al., 1981](#); [Ekström et al., 2012](#)). We first cor-
112 rected the instrument response, converted the waveform data into the displacement,
113 and applied a bandpass filter between 0.03 and 0.1 Hz. Second, we rotated the two
114 horizontal waveforms into the radial and transverse components based on the station
115 catalog information of horizontal orientation provided by IRIS DMC and AusPass. To
116 discard the low-quality data, we calculated signal-to-noise ratios (SNR) in the vertical
117 and radial components and removed data with vertical SNR < 5.0 or radial SNR $<$
118 3.0. Then, for each seismic event and station, we performed a time-domain complex
119 polarization analysis of [Vidale \(1986\)](#) to measure the horizontal arrival angles Θ of
120 direct P-waves in a similar way to [Yoshizawa et al. \(1999\)](#), which is summarized in
121 Figure 2. Since teleseismic P-wave is likely to linearly oscillate in the radial-vertical
122 plane, we imposed the data selection criteria on the ellipticity parameter P_E smaller
123 than 0.175. Third, we calculated the median of the time-dependent arrival angles for
124 each event (an orange line in the third panel in Figure 2 (a)) in a selected time win-
125 dow. In this study, we set the time window as 7.5 s before and after the main P-wave

126 pulse (Figure 2 (a)). Consequently, in the final step, we compiled a large number of
127 arrival angle data from many seismic events to evaluate the misorientation of hori-
128 zontal sensors. In this study, to reduce the influence of biased event distributions, we
129 mainly adopted the median as a representative measure for arrival-angle anomalies
130 (i.e., deviations from the great-circle direction) over the selected observation period
131 (Figure 2 (b)). Still, we also reported the mean values in our catalog (Tables S1–S3 and
132 Tarumi and Yoshizawa (2024)). We conducted this final step for stations with more
133 than 5 arrival-angle measurements, and discarded several stations with large uncer-
134 tainties in the time-dependent polarization data via visual inspections. The resultant
135 distribution of all employed events used in this study is shown in Figure 1 (c).

136 Station metadata (or reported catalog information of horizontal orientation) for
137 permanent stations is subject to change from time to time, reflecting irregular main-
138 tenance, calibrations, and replacement of instruments. For the permanent stations
139 with a long observation period, we visually inspected the timing of sudden changes in
140 the trend of estimated horizontal misorientation, allowing us to detect some temporal
141 changes at unreported timings (e.g., AU.COEN in Figure 3 (f)). For the estimation
142 of horizontal misorientation, we divide the period windows in which the median of
143 measured arrival angles is computed, depending on each station, as shown in Figures
144 2 (b) and 3.

145 3 Results

146 Our arrival-angle measurements enabled us to detect probable misorientations from
147 the geographic north for permanent and temporary stations (Figures 2, 3, 4, 5, and
148 S7). All results are summarized in Supplementary Materials 2 (Tables S1–S3) and
149 Zenodo Repository (Tarumi and Yoshizawa, 2024). In this section, we explain our
150 results on the permanent and temporary stations separately.

151 **3.1 Permanent Stations**

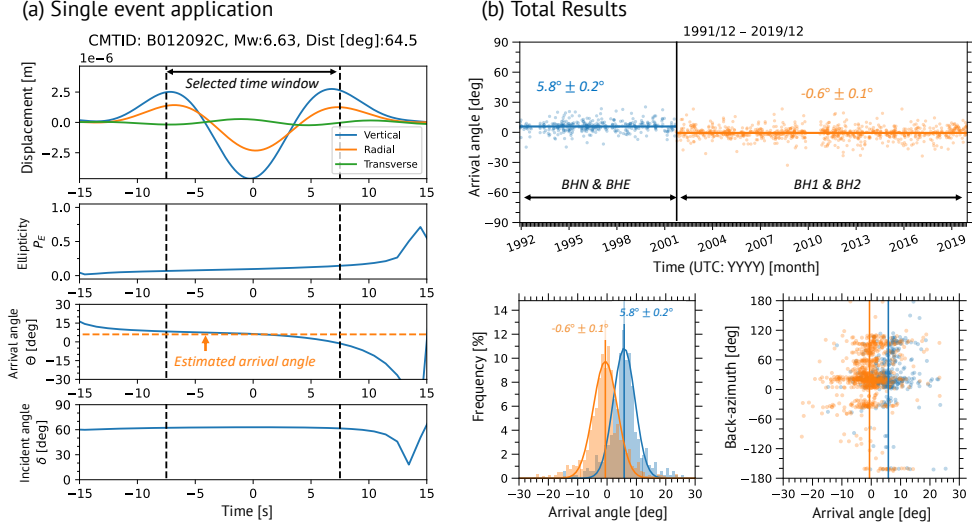


Fig. 2 A visual summary of P-wave polarization analysis for IU.NWAO. (a) An example of tele-seismic P-wave for an event at the epicentral distance of 64.5 degrees and the estimated polarization parameters. From top to bottom: three-component displacement waveforms rotated to the catalog values of IRIS metadata (blue: vertical; orange: radial; green: transverse), ellipticity P_E , arrival angle Θ on a horizontal plane, and incident angle δ for the P-wave particle motion. The arrival angle is measured clockwise from the radial (great-circle) direction so that a positive deviation indicates the arrival-angle anomaly to the east. In the third panel, a dashed orange line exhibits a median value in the selected time window encompassed by vertical dashed lines. (b) Compiled P-wave polarization data for all events used for the NWAO station. The top panel represents the time series of P-wave arrival angles. The colors for dots and lines represent the distinct period characterized by different trends of arrival angles. The timing of the arrival-angle trend change in September 2001 (indicated by a solid vertical line) matched well with the reported correction of horizontal components by IRIS. The bottom-left panel shows histograms and fitted Gaussian function for each period, and the bottom-right one indicates the back-azimuth dependence of the measured arrival angles for all employed events. In the top and bottom-left panels, the estimated station orientations and standard errors are labeled. The colors of the characters correspond to each distinct time period.

152 Figure 2 shows the summary of P-wave polarization measurements for IU.NWAO
 153 which has been a long-running station located in southeast Australia since 1992.
 154 According to the IRIS metadata catalog, the channel name of the horizontal compo-
 155 nents was changed from BHN/BHE to BH1/BH2 in September 2001. Our measured
 156 P-wave arrival angles show apparent temporal changes in the polarization trend at
 157 this time. The misorientation angle of horizontal sensors was estimated to be about

¹⁵⁸ 5.8° before September 2001, and it has decreased to 0.6° since then (by 2019, at least),
¹⁵⁹ indicating the improvement in the catalog information of this station.

¹⁶⁰ Note that, for this station, [Laske and Masters \(1996\)](#), [Yoshizawa et al. \(1999\)](#), and
¹⁶¹ [Schulte-Pelkum et al. \(2001\)](#), who employed the particle motion of either Rayleigh
¹⁶² wave or teleseismic P-wave before 2000, have already reported the misalignment from
¹⁶³ the north by around 5° . In particular, our estimated misorientation angle (5.8°) before
¹⁶⁴ September 2001 in Figure 2 (b) is very close to the estimated value by [Schulte-Pelkum](#)
¹⁶⁵ [et al. \(2001\)](#), who employed the P wave data in the same period. [Fontaine et al.](#)
¹⁶⁶ [\(2009\)](#) also used similar P-wave datasets and identified a misalignment of 5° , which
¹⁶⁷ is consistent with our results. For the other GSN stations used in this study, our esti-
¹⁶⁸ mated orientations are generally in agreement with the previously published catalog
¹⁶⁹ ([Ekström, 2008](#)).

¹⁷⁰ In addition to temporal changes, we can also see a back-azimuthal dependence in
¹⁷¹ the arrival-angle data (Figure 2 (b, bottom-right panel)). Such azimuthal variations
¹⁷² of arrival angles can also be observed at other stations, which may be worth further
¹⁷³ investigation in the future since they may reflect the lateral variations of heterogeneity
¹⁷⁴ and azimuthal anisotropy, including dipping interfaces, in the upper mantle beneath
¹⁷⁵ the seismic station ([Schulte-Pelkum et al., 2001](#); [Fontaine et al., 2009](#)).

¹⁷⁶ Figure 3 shows the summary of P-wave polarization data (arrival-angle anomalies
¹⁷⁷ from the great circle for each path) for six permanent and two temporary stations
¹⁷⁸ during their operation period until 2019. The horizontal-component channels of these
¹⁷⁹ stations have been reported as BHN/BHE since their installation. At G.CAN (Can-
¹⁸⁰ berra by GEOSCOPE; Figure 3 (a)), the station orientation estimated in this study
¹⁸¹ is nearly 0° (Tables S1–S3 in Supplementary Materials), suggesting that this seis-
¹⁸² mometer has been accurately oriented to the geographic north and east. AU.TOO
¹⁸³ (Figure 3 (b)) also shows no significant temporal changes, though our measurements

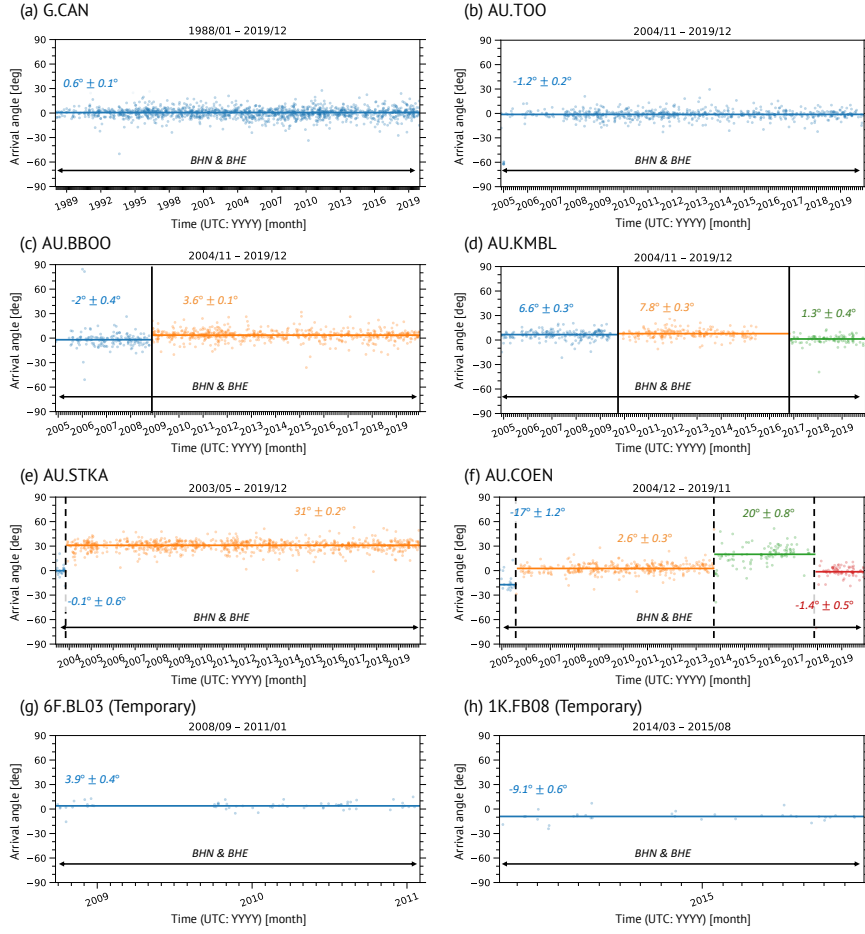


Fig. 3 Time-dependent P-wave polarization data (arrival-angle deviation from the great circle) for selected stations, (a-f) permanent stations installed and maintained by GEOSCOPE (G) and Geoscience Australia (AU), and (g, h) temporary stations. Notations in these figures are the same as 2 (b, top panel). The vertical black lines represent the timing of significant trend changes in P-wave arrival angles. Solid vertical lines indicate the timing of the reported maintenance and/or replacement of instruments, and dashed vertical lines represent unknown temporal changes at unreported timings. As described in the main text, we did not identify temporal change for temporary stations.

suggest a slight misalignment (about -1.2°) from the north which can be almost negligible. At AU.BBOO and AU.KMBL stations (Figure 3 (c, d)), we can see clear temporal changes in the trends of polarization angles, which coincide well with the timing of reported maintenance and/or instrument replacement. On the other hand,

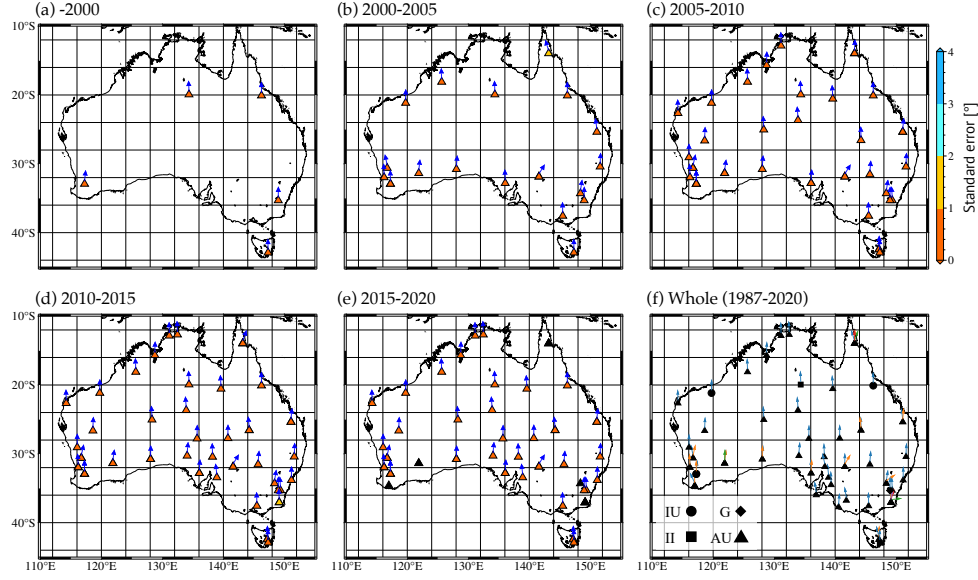


Fig. 4 Map projections of horizontal misorientations from the geographic north for permanent seismic stations (II, IU, G, and AU) in Australia. (a-e) Arrows indicate the median directions of horizontal sensors over the designated period. Colors in the triangles indicate the estimated standard errors shown in the color bar on the right. Black triangles without arrows indicate stations with varying misorientations during the period. (f) A compiled map of estimated misorientations for the whole period of analysis. The colors of arrows indicate the horizontal sensor orientations in different periods. Black symbols indicate stations of different seismic networks.

at AU.STKA and AU.COEN (Figure 3 (e, f)), unknown temporal changes in polarization angles are detected at unreported timings. In particular, STKA exhibits a very large misalignment from the north by 30° since the early stage of its operation.

Compiled maps of the estimated horizontal misorientations for permanent stations are displayed in Figure 4, in which we show the misorientations in each period in Figures 4 (a-e), and those compiled for the entire period of our analysis in Figure 4 (f). For permanent stations including those in the S1 network, the station misorientations and their standard errors are summarized in time-dependent horizontal bar graphs in Figures S1, S2, and S5 in Supplementary Material 1 (hereafter SM1) and are separately tabulated in Tables S1 and S2 in Supplementary Material 2 (hereafter SM2). In particular, we can identify significant time-dependent variations of misorientations for AU stations. These temporal changes mostly coincide with the reported

Table 1 Comparison of recent misalignment measurements at AU stations by [Eakin et al. \(2023\)](#) and this study. [Eakin et al. \(2023\)](#) estimated these using PKS and/or SKS phases, as indicated. In the third column showing our results, the data period and the number of seismic events used are shown (e.g., 2011–2019; 100).

Station	Eakin et al. (2023) (PKS and/or SKS)	This study (Teleseismic P-wave)
AU.ARPS	-6° (SKS)	-9.4°±4.4° (2019; 6)
AU.FORT	0° (PKS), 3.5° (SKS)	4.4°±0.4° (2003–2011; 69) 1.4°±0.2° (2011–2019; 404)
AU.HTT	-4° (PKS), -3° (SKS)	-6.3°±0.2° (2010–2019; 399)
AU.KELC	-6° (SKS)	-9°±1.3° (2019; 19)
AU.MGBR	-10° (SKS)	4.4°±1.8° (2019; 30)
AU.MILA	6° (SKS)	1.7°±0.6° (2011–2014; 44) -2.5°±1.6° (2014–2016; 22) 83°±0.9° (2016–2018; 18) 17°±1.1° (2018–2019; 17) 6.5°±1.0° (2019; 12)
AU.MULG	6.6° (PKS & SKS)	5.0°±0.4° (2013–2019; 219)
AU.SDAN	2.5° (SKS)	-1.5°±0.7° (2018–2019; 48)
AU.STKA	31° (PKS & SKS)	-0.1°±0.6° (2003; 23) 31.0°±0.2° (2003–2019; 899)
AU.YAPP	-13.4° (PKS & SKS)	-13°±0.5° (2018–2019; 55)
AU.YNG	5° (PKS), 10° (SKS)	8.7°±0.3° (2004–2017; 429) 56°±1.2° (2004–2017; 42)

200 timing of maintenance and/or replacement by the IRIS and AusPass. However, such
 201 temporal changes at several stations (e.g., AU.COEN) are found at unreported tim-
 202 ings. The misorientation of some permanent stations from the geographic north is
 203 more than 10°, which may affect seismic waveform analysis, especially when using the
 204 horizontal components. Figure S6 (SM1) demonstrates the three-component seismo-
 205 grams observed at STKA to compare waveforms before and after correcting the station
 206 misorientations. In Figure S6 (a) in SM1, we can see the apparent energy leakage of
 207 the P-wave from the radial to transverse component. In Section 4, we will discuss the
 208 effects of the station correction on azimuth-dependent receiver function analyses.

209 For AU stations, we compare our measurements with those from a recent study in
 210 Table 1; we present our estimated misalignments for selected AU stations, along with
 211 XKS-based measurements from [Eakin et al. \(2023\)](#). We focused on stations where
 212 [Eakin et al. \(2023\)](#) reported non-zero misalignments and extracted the most recent
 213 misorientation data from our catalog between 1987 and 2019 for comparison. Our

214 measurements are generally in good agreement with those of [Eakin et al. \(2023\)](#). Note
215 that large misalignments at AU.STKA are identical between both studies.

216 Figure S7 shows the map of station orientations for the S1 network (broadband seis-
217 mometers in schools; [Balfour et al., 2014](#)), which has been installed since 2011 ([Salmon](#)
218 [et al., 2011](#)). Table S2 in Supplementary Material 2 lists the estimated station orienta-
219 tions and their standard errors. Note that the lower corner-frequency of seismometers
220 (Güralp CMG-6TD) used for the S1 network ([Balfour et al., 2014](#)) is relatively high
221 (0.03Hz) compared to other permanent networks. Although we could obtain many
222 high-quality arrival-angle data when analyzing waveforms in the higher-frequency
223 range (e.g., 0.1–1.0 Hz), we could not gather sufficient arrival-angle measurements to
224 evaluate the station orientation for half of the S1 network since our current analysis
225 focuses on longer-period datasets (0.03–0.1 Hz). As a result, our S1 network catalog
226 (Table S2) includes only 13 stations (Figures S5 and S8).

227 3.2 Temporary Stations

228 The seismic records of temporary stations are generally less than two years long,
229 and we could not find any significant temporal changes in the horizontal orientation.
230 Figures 3 (g) and (h) show examples of a time-dependent polarization measurement
231 for selected temporary stations. As expected from the limited data acquisition period,
232 we could not observe any significant temporal changes in the time-series data of these
233 stations. In Figure 5, we compiled the station orientation for all temporary stations
234 that met the criteria described in Section 2. Also, we summarized the station orienta-
235 tions and their standard errors in Figures S3 and S4 and Table S3 in Supplemental
236 Materials. While some stations exhibit relatively large misalignments, the horizontal
237 sensors at almost all temporary stations generally align with the geographic north and
238 east directions (Figures 5 and S3), suggesting proper installation. We also compare

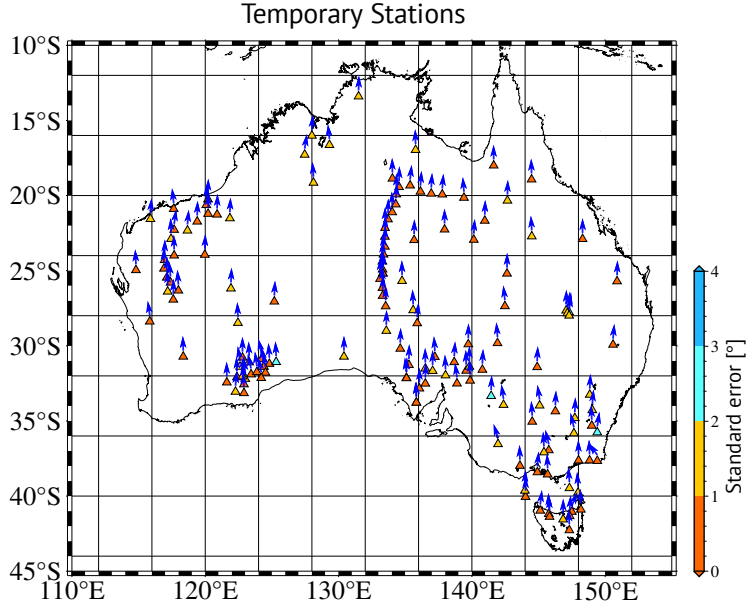


Fig. 5 Station misorientations from the geographic north in a horizontal sensor for temporary seismic stations.

XKS-based measurements from Eakin et al. (2023) and teleseismic P-wave measurements from this study in Table 2, similar to the previous subsection. Overall, for most temporary stations, our results are generally consistent with those of Eakin et al. (2023). The discrepancies at some stations may be attributed to the utilized recording periods, the measurement quality for different seismic phases, and the number of employed events.

4 Discussion and Conclusions

In this section, we briefly examine the effect of the station correction on P-wave receiver function (P-RF) analysis. We computed the P-RFs at AU.STKA, where a large misorientation of over 30° was observed, and analyzed the differences between uncorrected and corrected P-RF data for both radial and transverse components. In these calculations, we considered the azimuthal dependence of P-RFs, which arises from the varying incoming directions (or back-azimuths) of teleseismic P-wave. The

Table 2 Same as Table 1, but for selected temporary stations.

Station	Eakin et al. (2023) (PKS and/or SKS)	This study (Teleseismic P-wave)
1E.SQA01	5° (SKS)	3.0°±2.4° (2013–2014; 7)
1E.SQA09	10° (SKS)	16.0°±1.4° (2013–2014; 7)
1E.SQA11	10° (SKS)	9.2°±1.3° (2013–2014; 7)
1P.BA12	-25° (SKS)	-36.0°±0.9° (2011–2013; 9)
1P.BA13	0° (SKS)	-1.8°±0.8° (2011–2013; 26)
1P.BA19	9° (SKS)	-2.7°±0.8° (2011–2013; 16)
7H.TB03	5° (SKS)	-3.0°±1.0° (2011–2013)
7I.GA06	-5° (PKS), 0° (SKS)	-6.3°±0.9° (2004; 7)
7I.GA08	-5° (SKS)	-3.4°±0.9° (2004–2005; 10)
7I.TL10	-7° (PKS & SKS)	-6.1°±0.8° (2003–2005; 19)
7I.TL14	0° (PKS), 8° (SKS)	-4.4°±0.7° (2003–2005; 38)
7I.TL17	5° (SKS)	-1.4°±0.4° (2003–2005; 30)
7K.SOC03	0° (PKS), 5° (SKS)	2.7°±1.26° (2007–2008; 6)

azimuth-dependent radial P-RFs reflect lateral variations in seismic discontinuities around the station (e.g., [Tonegawa et al., 2005](#); [Kawakatsu et al., 2009](#); [Kumar and Kawakatsu, 2011](#)). In addition, incorporating transverse P-RFs enables us to infer seismic anisotropy in the crust and upper mantle (e.g., [Park and Levin, 2016](#); [Shiomi, 2017](#); [Birkey and Ford, 2023](#)). Significant uncertainties in the horizontal component orientations could lead to misinterpretations in the results of P-RF analysis.

Figure S6 in Supplementary Material 1 shows an example of teleseismic P-wave records observed at AU.STKA before and after the correction for station orientation, clearly indicating the energy leakage of P-wave from radial to transverse in the uncorrected horizontal traces. Using these two sets of teleseismic P-wave data, we computed radial and transverse P-RFs for two incoming directions within narrow distance ranges (10°) (Figure 6 (a, c)). After calculating individual P-RFs, we selected P-RF traces using the cross-correlation coefficient (CC)-based selection method ([Tkalcic et al., 2011](#)), stacking all traces with $CC > 0.7$. The resulting stacked P-RF traces are shown in Figure 6 (b, d), and the stacking process is visually summarized in Figures S8 and S9 in Supplementary Material 1. The radial P-RFs are generally consistent regardless of the correction of misorientation. Still, the relative amplitude of converted phases for the direct P-wave can be modulated, potentially affecting analyses that rely on

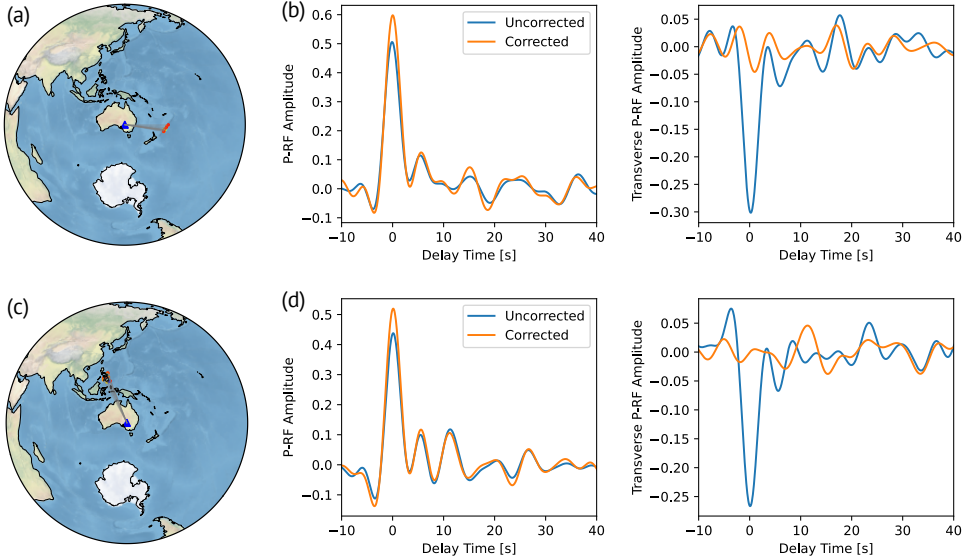


Fig. 6 Comparison of P-wave receiver functions (P-RFs) for AU.STKA. (a, c) Maps showing event groups used for the P-RF analysis. (b) Stacked radial and transverse P-RFs for the eastern events shown in (a). Blue and orange lines represent P-RFs from uncorrected and corrected teleseismic P-wave data, respectively. (d) Same as (b), but for the northwestern events shown in (c).

RF amplitude. For the transverse RFs, clear differences emerge between the uncorrected and corrected P-RF traces. In the uncorrected transverse P-RFs, we can see clear signals of direct P-wave, Moho-converted phases, and their multiple reflections, contaminating the P-to-SH converted phases. This contamination prevents us from properly interpreting P-to-SH conversions, which can be generated by anisotropic properties or oblique interfaces. Therefore, proper corrections of station azimuths during the waveform processing are essential for the accurate interpretation of both radial and transverse P-RF amplitudes.

In this study, we constructed a comprehensive station orientation catalog for Australian broadband seismic stations by analyzing long-period teleseismic P-wave particle motion data. The catalog includes temporal variations in station misorientations. While the timing of these changes is generally consistent with the published IRIS catalog, some stations exhibit changes at unexpected times. Finally, we assessed the utility

283 of our catalog in receiver function analysis, demonstrating that correcting for station
284 misorientation can significantly affect the amplitude analysis of RFs, particularly in
285 the transverse component.

286 References

- 287 Beyreuther, M., Barsch, R., Krischer, L., Megies, T., Behr, Y., Wassermann, J.:
288 ObsPy: A Python Toolbox for Seismology. *Seismological Research Letters* **81**(3),
289 530–533 (2010) <https://doi.org/10.1785/gssrl.81.3.530>
- 290 Birkey, A., Ford, H.A.: Anisotropic structure of the Australian continent. *Frontiers in*
291 *Earth Science* **10**, 1055480 (2023) <https://doi.org/10.3389/feart.2022.1055480>
- 292 Balfour, N.J., Salmon, M., Sambridge, M.: The Australian Seismometers in Schools
293 Network: Education, Outreach, Research, and Monitoring. *Seismological Research*
294 *Letters* **85**(5), 1063–1068 (2014) <https://doi.org/10.1785/0220140025>
- 295 Crampin, S.: Distinctive Particle Motion of Surface Waves as a Diagnostic of
296 Anisotropic Layering. *Geophysical Journal of the Royal Astronomical Society* **40**(2),
297 177–186 (1975) <https://doi.org/10.1111/j.1365-246x.1975.tb07045.x>
- 298 Crampin, S., Stephen, R.A., McGonigle, R.: The polarization of P-waves in anisotropic
299 media. *Geophysical Journal of the Royal Astronomical Society* **68**(2), 477–485
300 (1982) <https://doi.org/10.1111/j.1365-246x.1982.tb04910.x>
- 301 Dziewonski, A.M., Chou, T.A., Woodhouse, J.H.: Determination of earthquake source
302 parameters from waveform data for studies of global and regional seismicity. *Journal*
303 *of Geophysical Research: Solid Earth* **86**(B4), 2825–2852 (1981) <https://doi.org/10.1029/jb086ib04p02825>
- 305 Ekström, G., Busby, R.W.: Measurements of Seismometer Orientation at USArray

- 306 Transportable Array and Backbone Stations. Seismological Research Letters **79**(4),
307 554–561 (2008) <https://doi.org/10.1785/gssrl.79.4.554>
- 308 Eakin, C.M., Davies, D.R., Ghelichkhan, S., O'Donnell, J.P., Agrawal, S.: The Influ-
309 ence of Lithospheric Thickness Variations Beneath Australia on Seismic Anisotropy
310 and Mantle Flow. Geochemistry, Geophysics, Geosystems **24**(9) (2023) <https://doi.org/10.1029/2023gc011066>
- 312 Ekström, G., Dalton, C.A., Nettles, M.: Observations of Time-dependent Errors in
313 Long-period Instrument Gain at Global Seismic Stations. Seismological Research
314 Letters **77**(1), 12–22 (2006) <https://doi.org/10.1785/gssrl.77.1.12>
- 315 Ekström, G.: Polarization anomalies at various stations (2008). https://www.ldeo.columbia.edu/\texttildelowekstrom/Projects/WQC/COMB_QC/ Accessed 2024-
316 10-7
- 318 Ekström, G., Nettles, M., Dziewoński, A.M.: The global CMT project 2004–2010:
319 Centroid-moment tensors for 13,017 earthquakes. Physics of the Earth and Plane-
320 tary Interiors **200**, 1–9 (2012) <https://doi.org/10.1016/j.pepi.2012.04.002>
- 321 Fontaine, F.R., Barruol, G., Kennett, B.L.N., Bokelmann, G.H.R., Reymond, D.:
322 Upper mantle anisotropy beneath Australia and Tahiti from P wave polarization:
323 Implications for real-time earthquake location. Journal of Geophysical Research:
324 Solid Earth **114**(B3) (2009) <https://doi.org/10.1029/2008jb005709>
- 325 Fontaine, F., Kennet, B.: SOC - Southern Craton. International Federation of Digital
326 Seismograph Networks (2007). https://www.fdsn.org/networks/detail/7K_2007/
- 327 Hilst, R.v.d., Kennett, B.: SKIPPY. Australian Passive Seismic Server (1993). https://www.fdsn.org/networks/detail/7B_1993/

- 329 Hilst, R.v.d., Kennett, B., Christie, D., Grant, J.: Project Skippy explores lithosphere
330 and mantle beneath Australia. *Eos, Transactions American Geophysical Union*
331 **75**(15), 177–181 (1994) <https://doi.org/10.1029/94eo00857>
- 332 Hejrani, B., Tkalčić, H.: Resolvability of the Centroid-Moment-Tensors for Shallow
333 Seismic Sources and Improvements From Modeling High-Frequency Waveforms.
334 *Journal of Geophysical Research: Solid Earth* **125**(7) (2020) [https://doi.org/10.](https://doi.org/10.1029/2020jb019643)
335 [10.1029/2020jb019643](https://doi.org/10.1029/2020jb019643)
- 336 Hunter, J.D.: Matplotlib: A 2D Graphics Environment. *Computing in Science &*
337 *Engineering* **9**(3), 90–95 (2007) <https://doi.org/10.1109/mcse.2007.55>
- 338 Kennett, B., Debayle, E., Gorbatov, A.: QUOLL. International Federation of Digital
339 Seismograph Networks (1999). https://www.fdsn.org/networks/detail/7F_1999/
- 340 Kennett, B.: KIMBA97. International Federation of Digital Seismograph Networks
341 (1997). https://www.fdsn.org/networks/detail/7D_1997/
- 342 Kennett, B.: KIMBA98. International Federation of Digital Seismograph Networks
343 (1998). https://www.fdsn.org/networks/detail/7E_1998/
- 344 Kennet, B.: West Australian Cratons. International Federation of Digital Seismograph
345 Networks (2000). https://www.fdsn.org/networks/detail/7G_2000/
- 346 Kennett, B.: TASMAL. International Federation of Digital Seismograph Networks
347 (2003). https://www.fdsn.org/networks/detail/7I_2003/
- 348 Kennett, B.L.N., Furumura, T.: Stochastic waveguide in the lithosphere: Indonesian
349 subduction zone to Australian craton. *Geophysical Journal International* **172**(1),
350 363–382 (2008) <https://doi.org/10.1111/j.1365-246x.2007.03647.x>
- 351 Kennett, B.L.N., Fichtner, A., Fishwick, S., Yoshizawa, K.: Australian Seismological

- 352 Reference Model (AuSREM): mantle component. Geophysical Journal International
353 **192**(2), 871–887 (2013) <https://doi.org/10.1093/gji/ggs065>
- 354 Kumar, P., Kawakatsu, H.: Imaging the seismic lithosphere-asthenosphere boundary
355 of the oceanic plate. Geochemistry, Geophysics, Geosystems **12**(1), (2011) <https://doi.org/10.1029/2010gc003358>
- 357 Kawakatsu, H., Kumar, P., Takei, Y., Shinohara, M., Kanazawa, T., Araki, E., Suye-
358 hiro, K.: Seismic Evidence for Sharp Lithosphere-Asthenosphere Boundaries of
359 Oceanic Plates. Science **324**(5926), 499–502 (2009) <https://doi.org/10.1126/science.1169499>
- 361 Laske, G.: Global observation of off-great-circle propagation of Long-Period surface
362 waves. Geophysical Journal International **123**(1), 245–259 (1995) <https://doi.org/10.1111/j.1365-246x.1995.tb06673.x>
- 364 Larson, E.W.F., Ekström, G.: Determining surface wave arrival angle anomalies. Journal
365 of Geophysical Research **107**(B6) (2002) <https://doi.org/10.1029/2000jb000048>
- 366 Laske, G., Masters, G.: Constraints on global phase velocity maps from long-period
367 polarization data. Journal of Geophysical Research: Solid Earth **101**(B7), 16059–
368 16075 (1996) <https://doi.org/10.1029/96jb00526>
- 369 Met Office: Cartopy: a Cartographic Python Library with a Matplotlib Interface.
370 (2010). <https://scitools.org.uk/cartopy>
- 371 Miller, M.S.: Transitions in the Banda Arc-Australia continental collision. Interna-
372 tional Federation of Digital Seismograph Networks (2014). https://www.fdsn.org/networks/detail/1G_2019/
- 374 Park, J., Levin, V.: Anisotropic shear zones revealed by backazimuthal harmonics of

- 375 teleseismic receiver functions. *Geophysical Journal International* **207**(2), 1216–1243
376 (2016) <https://doi.org/10.1093/gji/ggw323>
- 377 Rawlinson, N., Kennett, B.: TIGGER BB. International Federation of Digital Seismo-
378 graph Networks (2001). https://www.fdsn.org/networks/detail/7H_2001/
- 379 Reading, A., Kennett, B.: CAPRA - Linkage. International Federation of Digital
380 Seismograph Networks (2005). https://www.fdsn.org/networks/detail/7J_2005/
- 381 Rawlinson, S., Kennet, B.: BILBY. Australian Passive Seismic Server (2008). https://www.fdsn.org/networks/detail/6F_2008/
- 382
- 383 Reading, A., Rawlinson, N.: Bass Strait. International Federation of Digital Seismo-
384 graph Networks (2011). https://www.fdsn.org/networks/detail/1P_2011/
- 385 Salmon, M., Balfour, N., Sambridge, M.: Australian Seismometers in Schools. AusPass
386 (2011). <https://www.fdsn.org/networks/detail/S1/>
- 387 Shioi, K.: Dissimilar receiver functions observed at very close stations in the Kii
388 Peninsula, central Japan: features and causes. *Earth, Planets and Space* **69**(1), 48
389 (2017) <https://doi.org/10.1186/s40623-017-0631-5>
- 390 Schulte-Pelkum, V., Masters, G., Shearer, P.M.: Upper mantle anisotropy from long-
391 period P polarization. *Journal of Geophysical Research: Solid Earth* **106**(B10),
392 21917–21934 (2001) <https://doi.org/10.1029/2001jb000346>
- 393 Tkalcic, H., Chen, Y., Liu, R., Zhibin, H., Sun, L., Chan, W.: Multistep modelling
394 of teleseismic receiver functions combined with constraints from seismic tomogra-
395 phy: crustal structure beneath southeast China. *Geophysical Journal International*
396 **187**(1), 303–326 (2011) <https://doi.org/10.1111/j.1365-246x.2011.05132.x>

- 397 Tonegawa, T., Hirahara, K., Shibusaki, T.: Detailed structure of the upper mantle dis-
398 continuities around the Japan subduction zone imaged by receiver function analyses.
399 Earth, Planets and Space **57**(1), 5–14 (2005) <https://doi.org/10.1186/bf03351801>
- 400 Tkalčić, H., Kennett, B., Sippl, C., Spaggiari, C., Gessner, K.: Albany-Fraser Experi-
401 ment. International Federation of Digital Seismograph Networks (2013). https://www.fdsn.org/networks/detail/1K_2013/
402
- 403 Tkalčić, H., Kennett, B., Tanaka, S., Stipčević, J.: Australia. Australian Passive
404 Seismic Server (2013). https://www.fdsn.org/networks/detail/1E_2013/
- 405 Tarumi, K., Yoshizawa, K.: Numerical Sheet for "Station-orientation catalog for
406 Australian broadband seismic stations". Zenodo (2024). <https://doi.org/10.5281/zenodo.13985090>
407
- 408 Uieda, L., Tian, D., Leong, W.J., Jones, M., Schlitzer, W., Toney, L., Grund, M.,
409 Yao, J., Magen, Y., Materna, K., Newton, T., Anant, A., Ziebarth, M., Wessel,
410 P., Quinn, J.: PyGMT: A Python interface for the Generic Mapping Tools (2021)
411 <https://doi.org/10.5281/zenodo.5607255> . The development of PyGMT has been
412 supported by NSF grants OCE-1558403 and EAR-1948603.
- 413 Vidale, J.E.: Complex polarization analysis of particle motion. Bulletin of the Seis-
414 mological Society of America **76**(5), 1393–1405 (1986) <https://doi.org/10.1785/bssa0760051393>
415
- 416 Wessel, P., Luis, J.F., Uieda, L., Scharroo, R., Wobbe, F., Smith, W.H.F., Tian,
417 D.: The Generic Mapping Tools Version 6. Geochemistry, Geophysics, Geosystems
418 **20**(11), 5556–5564 (2019) <https://doi.org/10.1029/2019gc008515>
- 419 Yoshizawa, K.: Radially anisotropic 3-D shear wave structure of the Australian litho-
420 sphere and asthenosphere from multi-mode surface waves. Physics of the Earth and

⁴²¹ Planetary Interiors **235**, 33–48 (2014) <https://doi.org/10.1016/j.pepi.2014.07.008>

⁴²² Yoshizawa, K., Yomogida, K., Tsuboi, S.: Resolving power of surface wave polarization data for higher-order heterogeneities. Geophysical Journal International **138**(1),
⁴²³ 205–220 (1999) <https://doi.org/10.1046/j.1365-246x.1999.00861.x>

⁴²⁵ Acknowledgment

⁴²⁶ All seismograms used in this study were obtained from the IRIS Data Management
⁴²⁷ Center (<https://ds.iris.edu/ds/nodes/dmc/>). We used ObsPy ([Beyreuther et al., 2010](#))
⁴²⁸ for downloading and analyzing all seismic waveform data. We used matplotlib ([Hunter, 2007](#)), cartopy ([Met Office, 2010](#)), Generic Mapping Tools ([Wessel et al., 2019](#)), and
⁴²⁹ PyGMT ([Uieda et al., 2021](#)) to create all figures.

⁴³¹ Data Availability

⁴³² The numerical data of our station misorientation catalog are included in PDF files
⁴³³ provided as a part of Supplementary Materials and Zenodo Repository ([Tarumi and](#)
⁴³⁴ [Yoshizawa, 2024](#)). All teleseismic waveform data used in this study are available
⁴³⁵ from the IRIS Data Management Center (<https://ds.iris.edu/ds/nodes/dmc/>) and the
⁴³⁶ Australian Passive Seismic Server (AusPass; <https://auspass.edu.au/index.html>).

⁴³⁷ Funding

⁴³⁸ This study was partly supported by JST SPRING grant number JPMJSP2119 to KT
⁴³⁹ and JSPS KAKENHI (grand number 24KJ0294 to KT; 20K04096 and 23K03539 to
⁴⁴⁰ KY).

⁴⁴¹ Competing Interests

⁴⁴² The authors have no relevant financial or non-financial interests to disclose.

⁴⁴³ **Author Contributions**

⁴⁴⁴ KT: Conceptualization, Data curation, Methodology, Formal analysis, Funding
⁴⁴⁵ acquisition, Investigation, Visualization, Software, Writing - Original draft; KY:
⁴⁴⁶ Conceptualization, Data curation, Methodology, Funding acquisition, Investigation,
⁴⁴⁷ Supervision, Project Administration, Writing – review and editing

Supplementary Material 1 for
**Station-orientation catalog for Australian broadband seismic
stations**

K. Tarumi^{1,*} and K. Yoshizawa^{1,2}

5 ¹ Department of Natural History Sciences, Graduate School of Science, Hokkaido University, Sapporo 060-0810, Japan

²Department of Earth & Planetary Sciences, Faculty of Science, Hokkaido University, Sapporo 060-0810, Japan.

*Corresponding author: tarumi.kotaro.jp@gmail.com

10

Supplementary Material 1 (this file) includes additional supporting figures (Figures S1-S9)

referred to in the main text. The station orientation catalogs for permanent and temporary stations are summarized separately in Supplementary Materials 2 (a separate PDF file), which includes detailed summary tables of our polarization analysis. As demonstrated in

15 the main text, the station orientation depends on the observation period, so we identified the timing of temporal changes by visually checking the time series of P-wave polarization data for each station. The start and end times indicate the initial and final dates for estimating the median angles. Following is a summary of the contents of Supplementary Materials.

- 20 • Figures S1–S5: Summary of time-dependent station orientation and the corresponding standard errors. Figures S1 and S2 show the results for permanent stations except for the *S1* network, Figures S3 and S4 for temporary stations, and Figure S5 for the *S1* network.
- 25 • Figure S6: An example of three-component P waveforms with or without the correction for horizontal misorientation at the AU.STKA station.
- Figure S7: A map projection of station misorientations from the geographic north for the *S1* network stations.
- Figure S8: Examples of P-wave receiver functions at AU.STKA using the eastern seismic events.

- 30 • Figure S9: Examples of P-wave receiver functions at AU.STKA using the western seismic events.

Note that Supplementary Material 2 (another PDF) includes the station orientation catalog (Tables S1–S3).

Clockwise misorientation from the north for Permanent Stations (AU / G / II / IU)

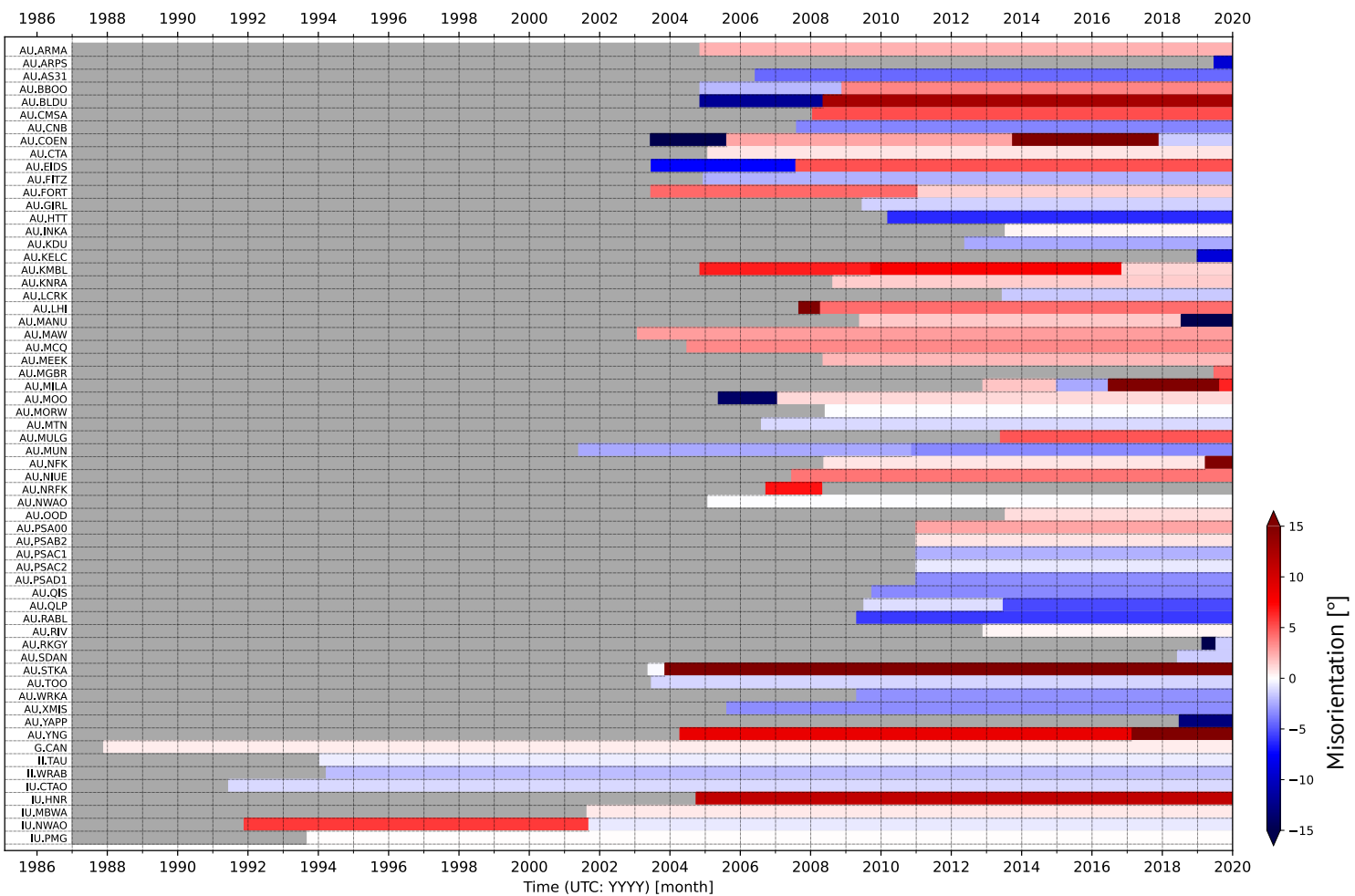


Figure S1. Summary of clockwise misorientation from the geographic north for permanent

35 stations (except for the *SI* network). A positive misorientation value represents the eastward rotation of horizontal sensors from the north. The gray region represents the period when the seismic station has not been operated. Note the operation periods for some stations (AU.ARPS, AU.KELC, AU.MGBR, AU.RKGY, and AU.SDAN) are too short to estimate the proper misorientation in our polarization analysis; see Supplementary Material

40 2 for details.

Standard errors of misorientation values for Permanent Stations (AU / G / II / IU)

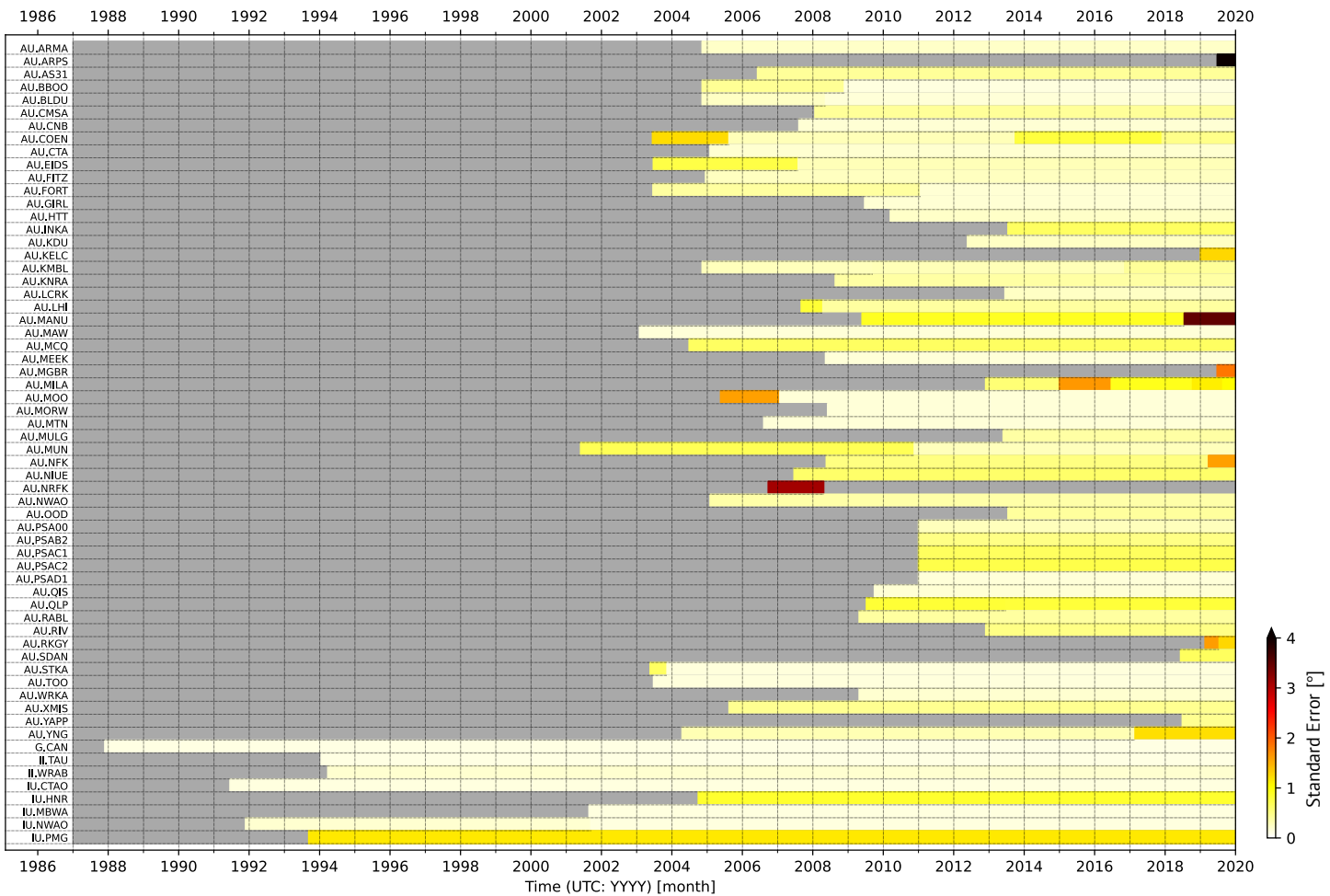


Figure S2. Same as Figure S1, but the summary of standard errors for the estimated misorientation values.

Clockwise misorientation from the north for Temporary stations

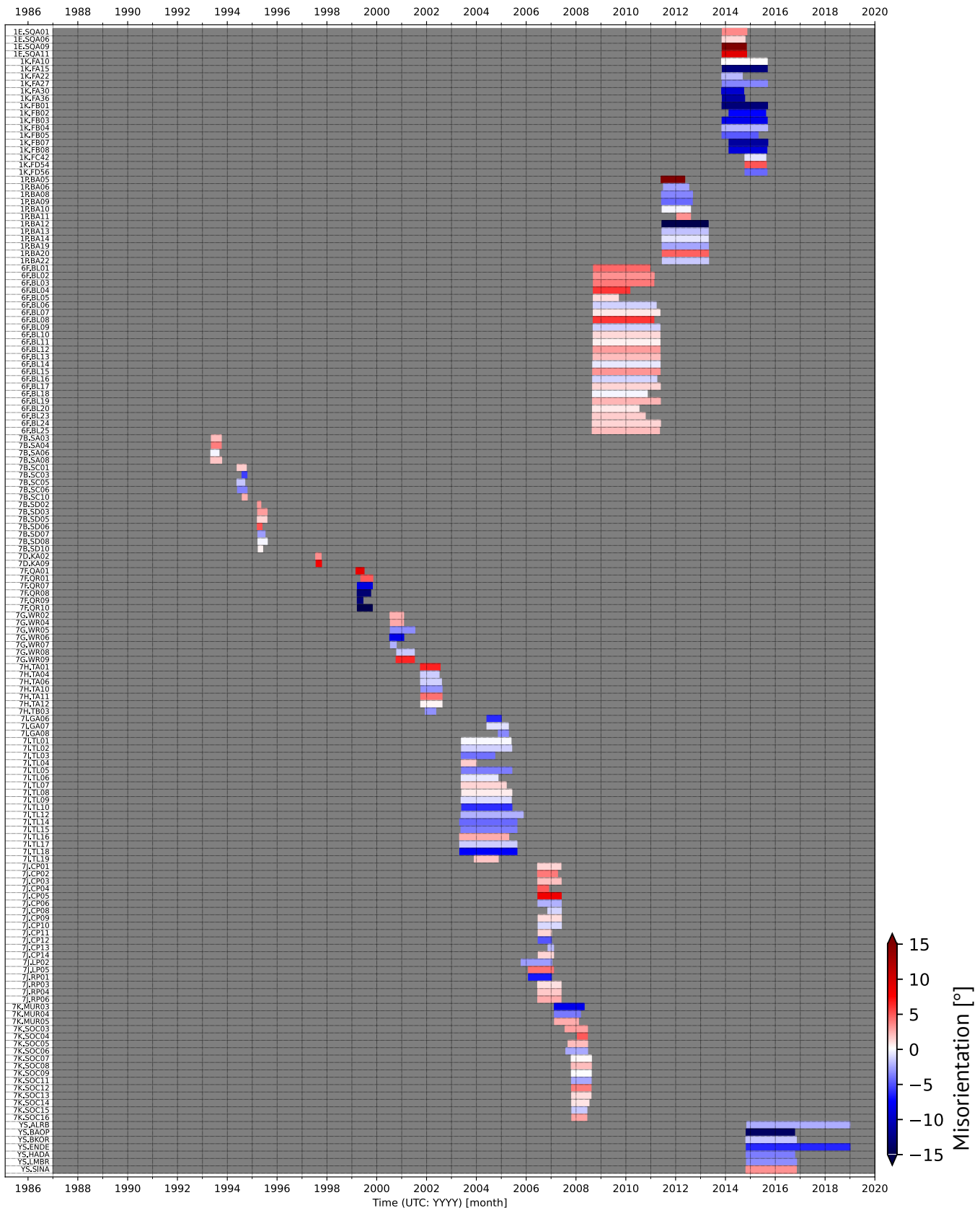


Figure S3: Same as Figure S1, but for the temporary stations.

Standard errors of misorientation values for Temporary stations

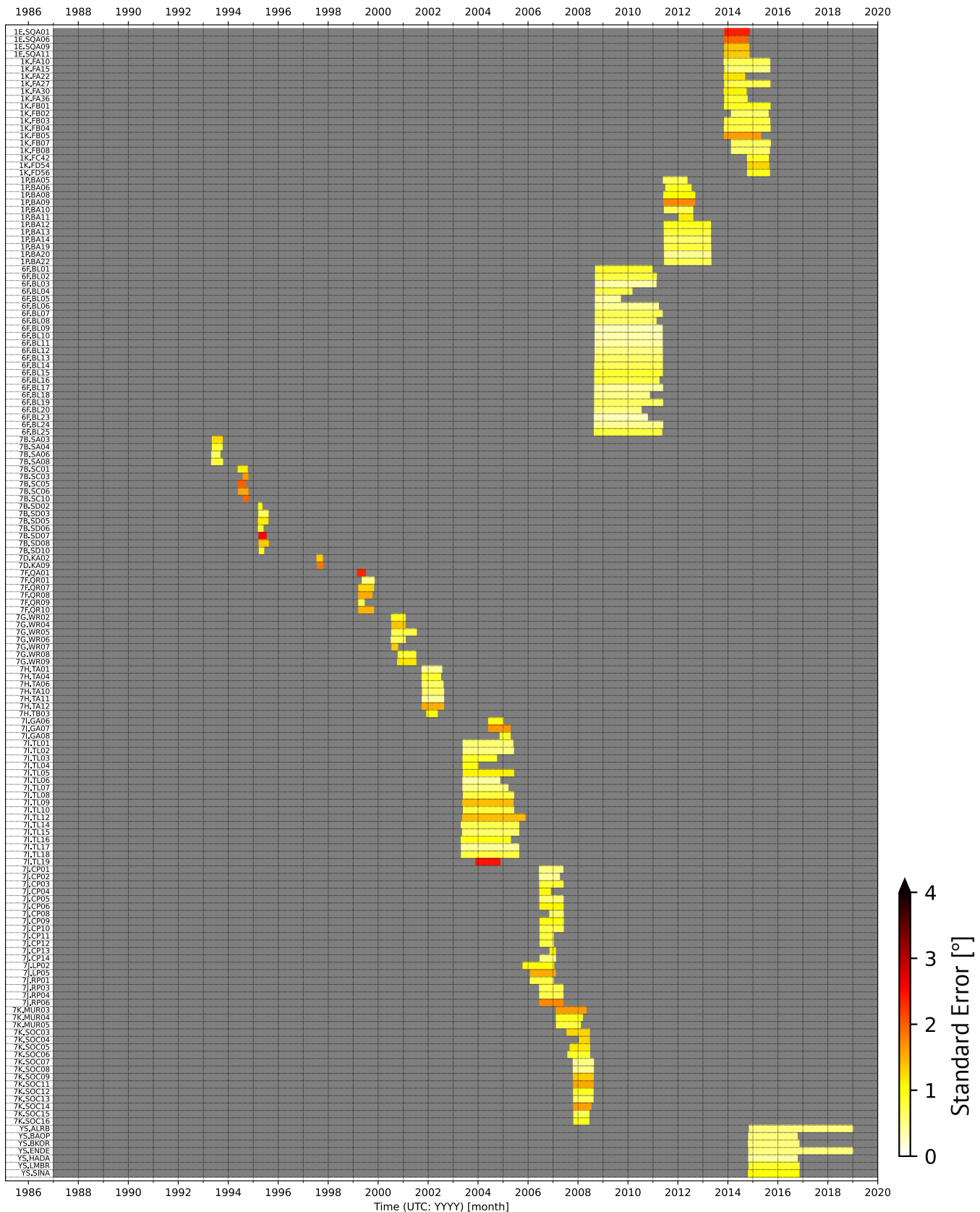
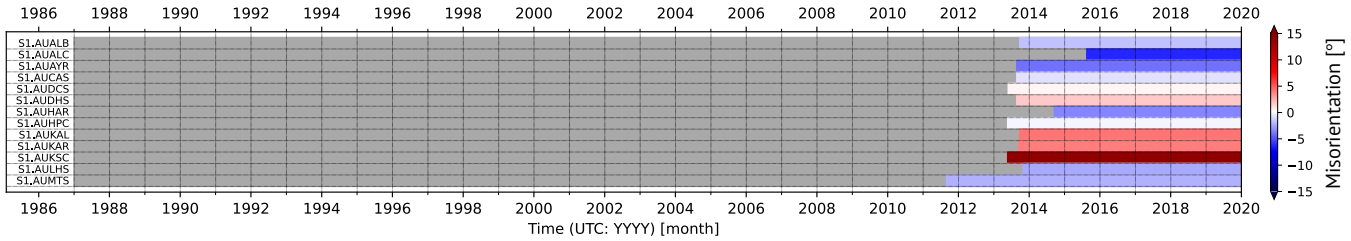


Figure S4: Same as Figure S2, but for the temporary stations.

Summary of S1 Stations

(a) Misorientation



(b) Standard error

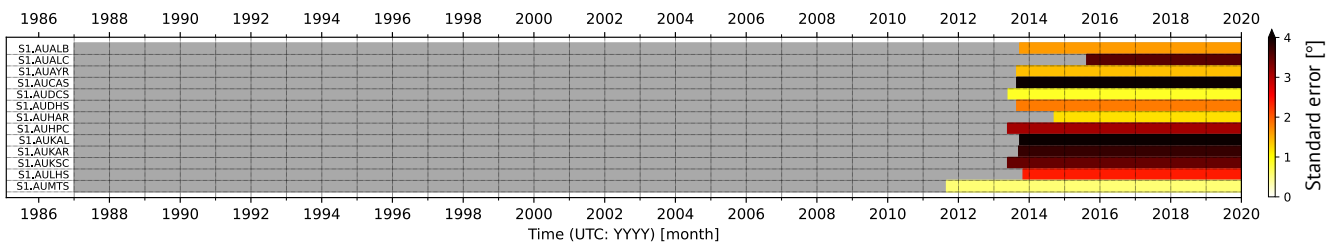
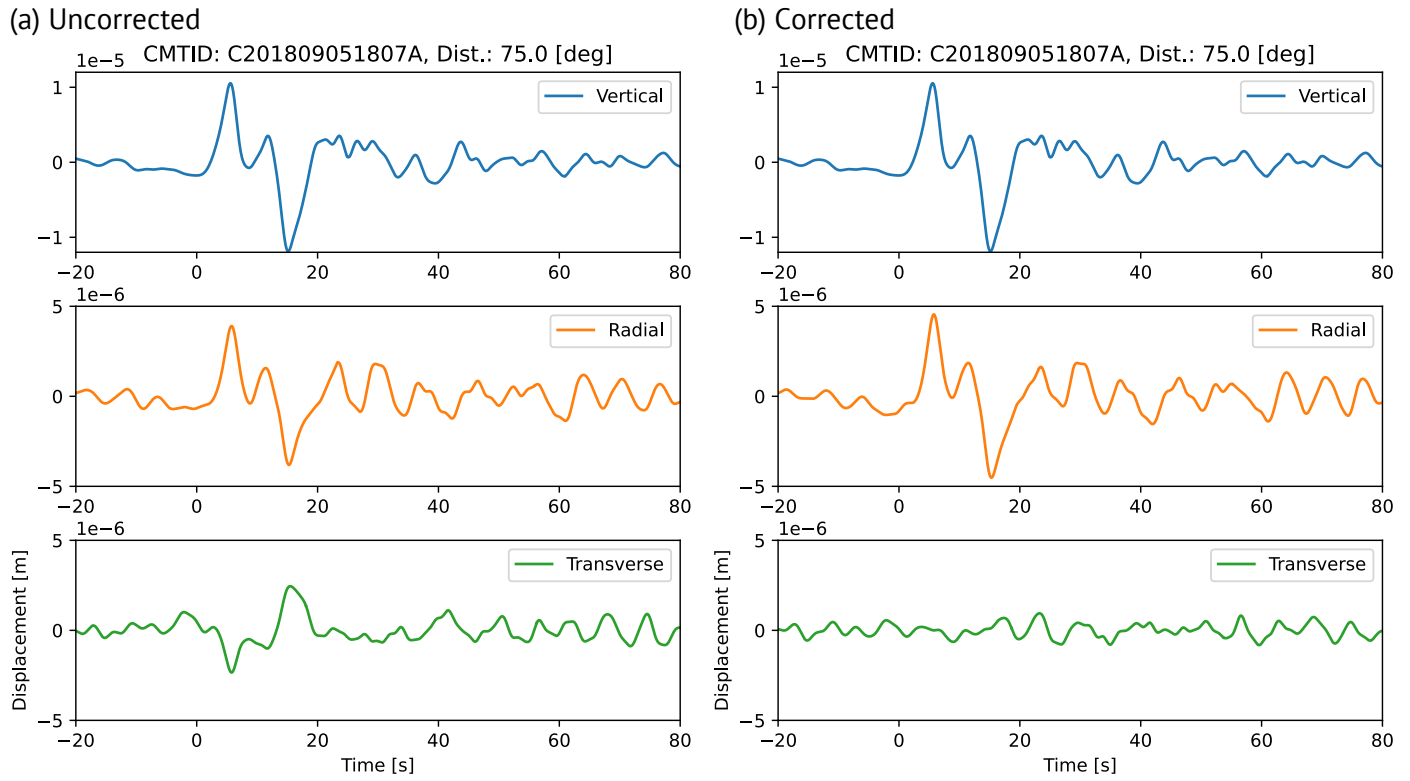


Figure S5: Summary of the *S1* network stations. (a) and (b) are the same as Figures S1 and S2, respectively, but for the *S1* network.



50 Figure S6: An example of teleseismic P-wave at AU.STKA for a seismic event (Mw 6.6)
 in Hokkaido, Japan, on September 5, 2018 (UTC). Three-component seismograms (a)
 before the correction of the station misorientation, and (b) after the correction. Blue, orange,
 and green lines indicate the vertical, radial, and transverse components. For the uncorrected
 waveforms in (a), we used the horizontal orientation reported by IRIS/AusPass, while for
 55 (b), we employed our new catalog of misorientation. Note that the amplitude scale in the
 top panel (vertical) is different from the other two horizontal components.

S1 Network

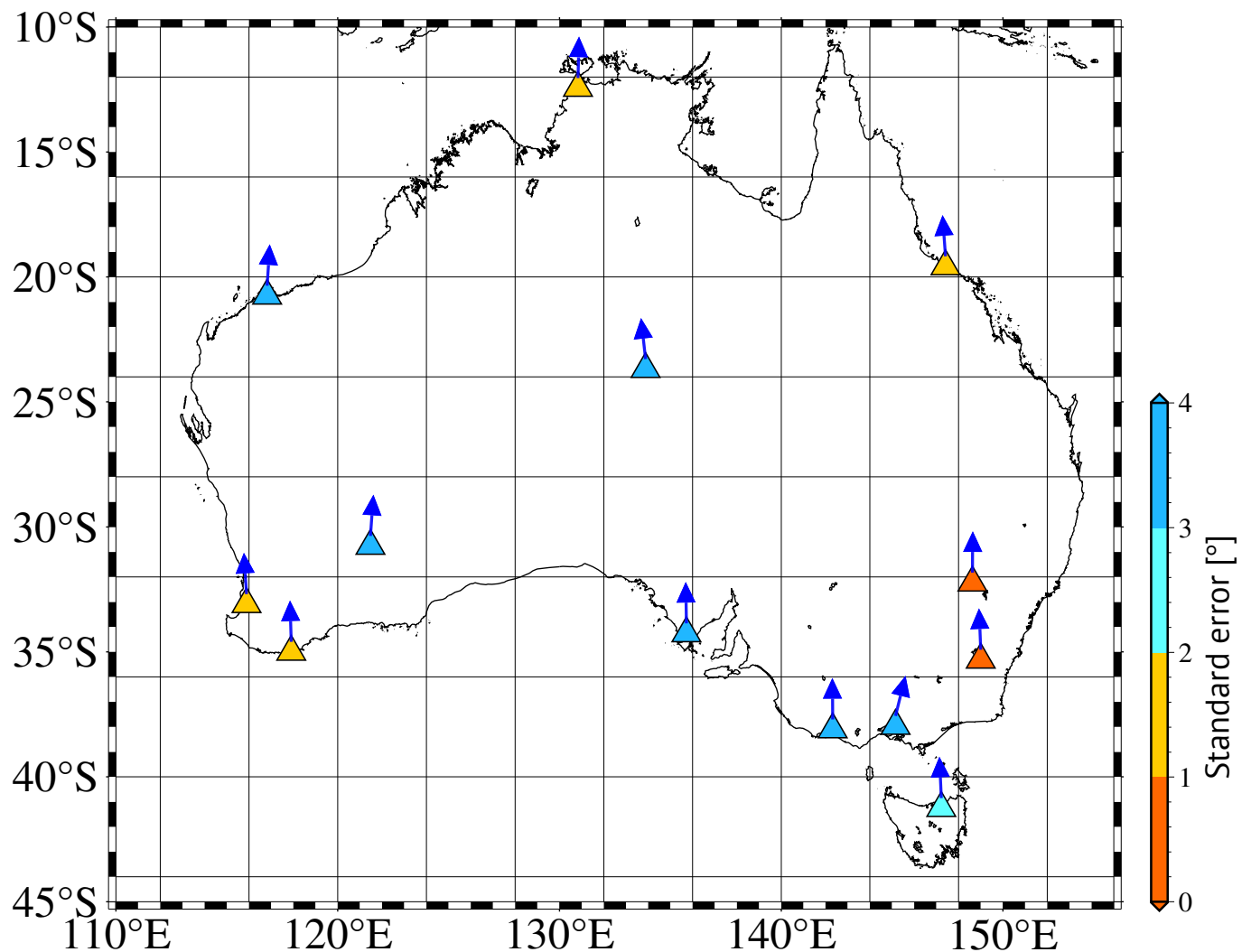


Figure S7: Same as Figures 4 (a-e) and 5 in the main text, but for the *S1* network.

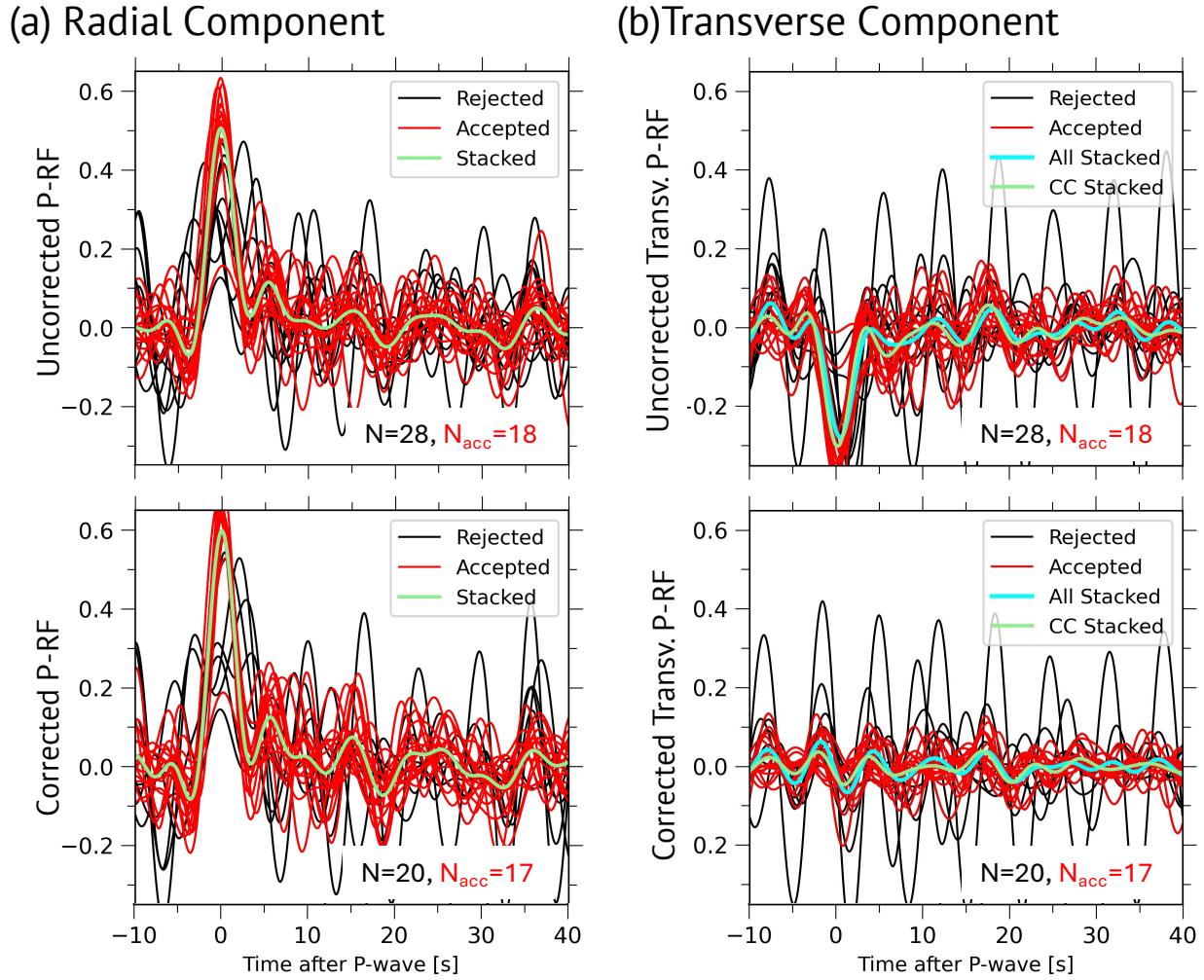
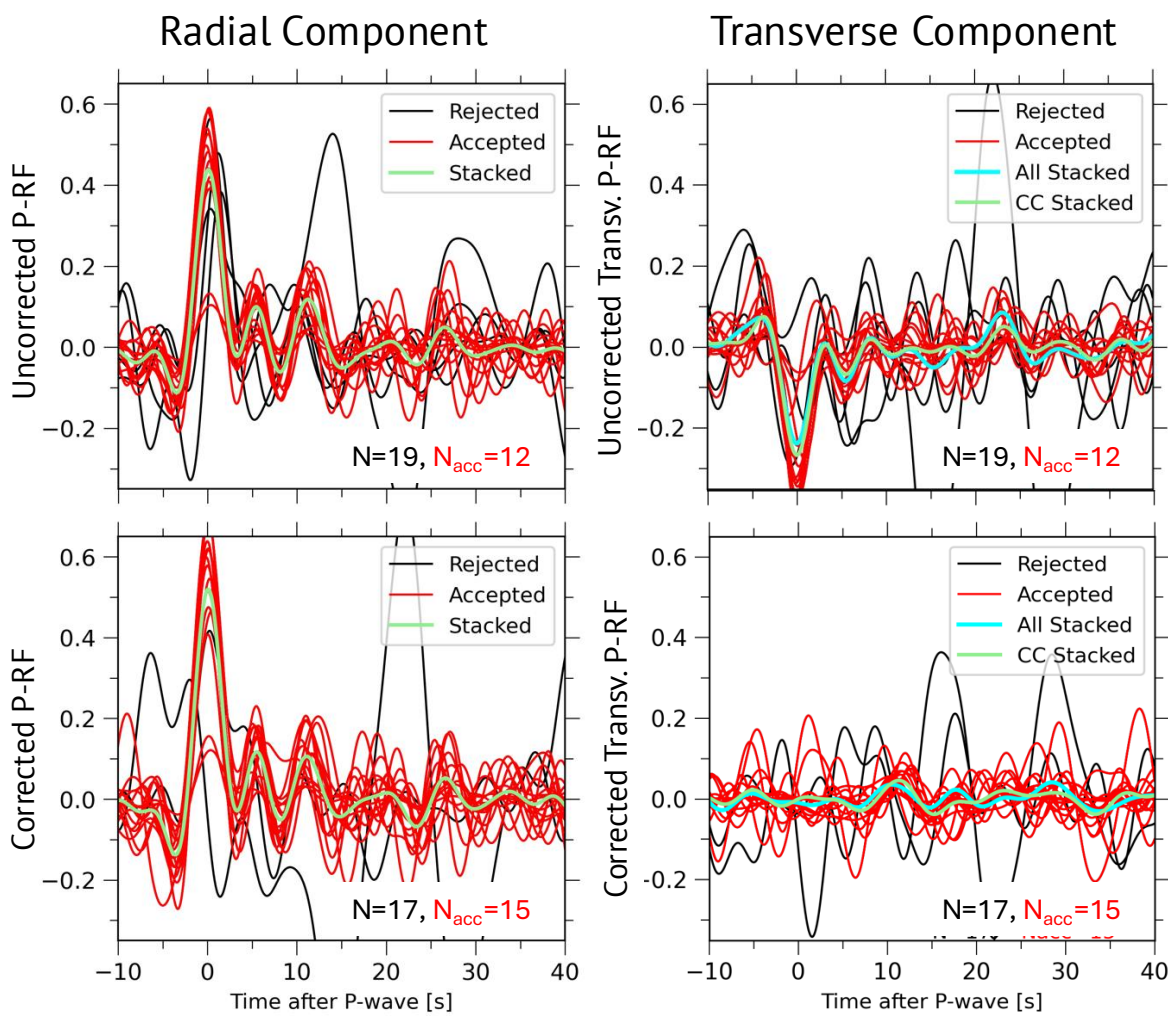


Figure S8: Examples of individual and stacked traces of P-wave receiver functions from
60 the eastern event groups at AU.STKA shown in Figure 5. (a) P-RFs in radial component
and (b) transverse component; (top) without and (bottom) with a correction for the station
misorientation. Black and red lines are the rejected and accepted traces, respectively,
through the cross-correlation-based selection step explained in the main text. Green traces
represent the stacked traces, shown as the blue or orange line in Figure 5b.



65 Figure S9: Same as Figure S8, but the P-wave receiver functions from the western event groups.

1 *Supplementary Material 2 for*

2 **Station-orientation catalog for Australian broadband seismic stations**

3 K. Tarumi^{1,*} and K. Yoshizawa^{1,2}

4 ¹ Department of Natural History Sciences, Graduate School of Science, Hokkaido University, Sapporo 060-
5 0810, Japan

6 ²Department of Earth & Planetary Sciences, Faculty of Science, Hokkaido University, Sapporo 060-0810,
7 Japan.

8 *Corresponding author: tarumi.kotaro.jp@gmail.com

9

10 Supplementary Material 2 (this file) includes additional supporting tables referred to in
11 the main text. Table S1 represents a station orientation catalog for permanent stations
12 except for the *S1* network. Details of tabulated parameters are summarized in the caption
13 in Table S1. Tables S2 and S3 are the same as Table S1 but for the *S1* network and
14 temporary stations, respectively.

15 Contents of this file:

- 16 ● Table S1: A Station orientation catalog for permanent stations except for the *S1* network.
17 ● Table S2: A Station orientation catalog for the *S1* network.
18 ● Table S3: A Station orientation catalog for temporary stations.

19

20

21 Table S1: Station orientation catalog for permanent stations except for the *SI* network.
 22 The first column includes the network code and station name. The second and third
 23 columns represent the period (start and end time) for calculating two statistical values
 24 (the median and mean) on station orientation (in the fourth and fifth columns, respectively)
 25 and its standard errors from the sixth column. The last column indicates the number of
 26 earthquakes used to estimate the misorientation during the designated period.

Network.Station	Start Time	End Time	Median [deg]	Mean [deg]	Std_err [deg]	N_{ev}
AU.ARMA	2004-11-09T21:48:34.105000Z	2019-12-31T23:59:59.000000Z	2.28	2.55	0.22	588
AU.ARPS	2019-06-25T00:00:00.000000Z	2019-12-31T23:59:59.000000Z	-9.37	-7.47	4.36	6
AU.AS31	2006-06-07T05:38:00.000000Z	2019-12-31T23:59:59.000000Z	-4.35	-5.19	0.42	561
AU.BBOO	2004-11-09T21:48:37.220000Z	2008-11-24T00:00:00.000000Z	-2	-1.45	0.43	159
AU.BBOO	2008-11-24T00:00:00.000000Z	2019-12-31T23:59:59.000000Z	3.62	3.53	0.14	652
AU.BLDU	2004-11-09T21:48:33.800000Z	2008-05-12T00:00:00.000000Z	-11.88	-11.94	0.24	142
AU.BLDU	2008-05-12T00:00:00.000000Z	2019-12-31T23:59:59.000000Z	12.72	11.86	0.16	657
AU.CMSA	2008-01-23T00:00:00.000000Z	2019-12-31T23:59:59.000000Z	5.16	4.02	0.42	508
AU.CNB	2007-08-10T02:32:30.594500Z	2019-12-31T23:59:59.000000Z	-3.55	-3.43	0.18	645
AU.COEN	2003-06-14T00:00:00.000000Z	2005-08-15T00:00:00.000000Z	-17.24	-13.51	1.23	20
AU.COEN	2005-08-15T00:00:00.000000Z	2013-10-01T00:00:00.000000Z	2.62	2.82	0.29	333
AU.COEN	2013-10-01T00:00:00.000000Z	2017-12-01T00:00:00.000000Z	19.97	19.35	0.78	104
AU.COEN	2017-12-01T00:00:00.000000Z	2019-12-31T23:59:59.000000Z	-1.41	-1.73	0.47	81
AU.CTA	2005-01-31T00:00:00.000000Z	2019-12-31T23:59:59.000000Z	0.81	0.87	0.19	538
AU.EIDS	2003-06-23T00:00:00.019500Z	2007-08-03T00:00:00.000000Z	-7.39	-12.19	0.74	130
AU.EIDS	2007-08-03T00:00:00.000000Z	2019-12-31T23:59:59.000000Z	5.09	4.06	0.29	534
AU.FITZ	2004-12-15T00:00:00.000000Z	2019-12-31T23:59:59.000000Z	-2.27	-2.02	0.25	427
AU.FORT	2003-06-19T00:00:00.000000Z	2011-01-23T00:00:00.000000Z	4.36	2.05	0.38	69
AU.FORT	2011-01-23T00:00:00.000000Z	2019-12-31T23:59:59.000000Z	1.37	1.36	0.18	404
AU.GIRL	2009-06-22T00:00:00.000000Z	2019-12-31T23:59:59.000000Z	-1.38	-1.27	0.18	373
AU.HTT	2010-03-15T00:00:00.000000Z	2019-12-31T23:59:59.000000Z	-6.29	-6.61	0.23	399

AU.INKA	2013-07-17T00:00:00.000000Z	2019-12-31T23:59:59.000000Z	0.27	0.29	0.63	37
AU.KDU	2012-05-23T00:00:00.000000Z	2019-12-31T23:59:59.000000Z	-2.57	-2.83	0.24	311
AU.KELC	2019-01-01T00:00:00.000000Z	2019-12-31T23:59:59.000000Z	-9.05	-9.13	1.26	19
AU.KMBL	2004-11-09T21:48:40.360000Z	2009-09-17T00:00:00.000000Z	6.62	6.39	0.28	202
AU.KMBL	2009-09-17T00:00:00.000000Z	2016-11-09T00:00:00.000000Z	7.81	7.71	0.29	203
AU.KMBL	2016-11-09T00:00:00.000000Z	2019-12-31T23:59:59.000000Z	1.28	0.72	0.41	93
AU.KNRA	2008-08-21T00:00:00.000000Z	2019-12-31T23:59:59.000000Z	1.5	0.31	0.37	356
AU.LCRK	2013-06-16T00:00:00.000000Z	2019-12-31T23:59:59.000000Z	-1.57	-2.09	0.24	252
AU.LHI	2007-09-03T04:36:09.594500Z	2008-04-15T00:00:00.000000Z	31.47	29.09	0.81	16
AU.LHI	2008-04-15T00:00:00.000000Z	2019-12-31T23:59:59.000000Z	4.3	4.7	0.39	117
AU.MANU	2009-05-26T00:00:00.000000Z	2018-07-18T00:00:00.000000Z	1.62	2.36	0.89	107
AU.MANU	2018-07-18T00:00:00.000000Z	2019-12-31T23:59:59.000000Z	-27.05	-22.03	3.47	18
AU.MAW	2003-01-31T00:00:00.000000Z	2019-12-31T23:59:59.000000Z	2.89	2.88	0.16	666
AU.MCQ	2004-06-28T00:00:00.000000Z	2019-12-31T23:59:59.000000Z	3.42	3.74	0.64	44
AU.MEEK	2008-05-12T00:00:00.000000Z	2019-12-31T23:59:59.000000Z	2.08	2.22	0.17	574
AU.MGBR	2019-06-24T00:11:23.600000Z	2019-12-31T23:59:59.000000Z	4.37	2.07	1.83	30
AU.MILA	2012-11-27T00:00:00.000000Z	2014-12-31T00:00:00.000000Z	1.68	0.89	0.55	44
AU.MILA	2014-12-31T00:00:00.000000Z	2016-06-22T00:00:00.000000Z	-2.51	-2.04	1.63	22
AU.MILA	2016-06-22T00:00:00.000000Z	2018-10-12T00:00:00.000000Z	82.67	73.93	0.92	18
AU.MILA	2018-10-12T00:00:00.000000Z	2019-08-21T23:59:59.000000Z	16.74	21.25	1.11	17
AU.MILA	2019-08-21T23:59:59.000000Z	2019-12-31T23:59:59.000000Z	6.45	7.7	1.02	12
AU.MOO	2005-05-20T01:36:40.000000Z	2007-01-25T00:00:00.000000Z	-13.84	-20.37	1.58	21
AU.MOO	2007-01-25T00:00:00.000000Z	2019-12-31T23:59:59.000000Z	1.09	0.6	0.16	530
AU.MORW	2008-06-03T00:05:17.594500Z	2019-12-31T23:59:59.000000Z	-0.08	0.35	0.17	665
AU.MTN	2006-08-11T00:00:00.000000Z	2019-12-31T23:59:59.000000Z	-1.09	-0.86	0.16	650
AU.MULG	2013-05-28T00:00:00.000000Z	2019-12-31T23:59:59.000000Z	4.99	4.6	0.36	219
AU.MUN	2001-05-30T00:00:00.000000Z	2010-11-18T00:00:00.000000Z	-2.47	-6.04	0.68	110
AU.MUN	2010-11-18T00:00:00.000000Z	2019-12-31T23:59:59.000000Z	-3.41	-3.55	0.28	424
AU.NFK	2008-05-20T00:00:00.000000Z	2019-03-26T05:26:20.000000Z	0.81	0.45	0.5	150
AU.NFK	2019-03-26T05:26:20.000000Z	2019-12-31T23:59:59.000000Z	40.39	39.78	1.58	9
AU.NIUE	2007-06-21T00:00:00.000000Z	2019-12-31T23:59:59.000000Z	4.02	2.76	0.6	123
AU.NRFK	2006-09-26T00:00:00.000000Z	2008-4-23T00:00:00.000000Z	6.92	17.61	3.08	15

AU.NWAO	2005-01-31T13:00:00.000000Z	2019-12-31T23:59:59.000000Z	-0.07	0.21	0.35	171
AU.OOD	2013-07-17T00:00:00.000000Z	2019-12-31T23:59:59.000000Z	0.99	2.05	0.4	251
AU.PSA00	2011-01-01T00:00:00.000000Z	2019-12-31T23:59:59.000000Z	2.6	3.01	0.28	234
AU.PSAB2	2011-01-01T00:00:00.000000Z	2019-12-31T23:59:59.000000Z	0.8	0.8	0.49	71
AU.PSAC1	2011-01-01T00:00:00.000000Z	2019-12-31T23:59:59.000000Z	-2.29	-2.7	0.65	75
AU.PSAC2	2011-01-01T00:00:00.000000Z	2019-12-31T23:59:59.000000Z	-0.69	-2.17	0.72	45
AU.PSAD1	2011-01-01T00:00:00.000000Z	2019-12-31T23:59:59.000000Z	-3.35	-3.46	0.16	279
AU.QIS	2009-10-01T00:00:00.000000Z	2019-12-31T23:59:59.000000Z	-3.41	-2.56	0.18	447
AU.QLP	2009-07-10T00:00:00.000000Z	2013-06-26T00:00:00.000000Z	-0.99	-0.89	0.81	62
AU.QLP	2013-06-26T00:00:00.000000Z	2019-12-31T23:59:59.000000Z	-5.36	-6.9	0.79	40
AU.RABL	2009-04-26T00:00:00.000000Z	2019-12-31T23:59:59.000000Z	-5.78	-3.72	0.38	271
AU.RIV	2012-11-28T00:00:00.000000Z	2019-12-31T23:59:59.000000Z	0.34	0.3	0.49	76
AU.RKGY	2019-02-19T00:00:00.000000Z	2019-07-15T00:00:00.000000Z	-25.1	-25.28	1.6	9
AU.RKGY	2019-07-15T00:00:00.000000Z	2019-12-31T23:59:59.000000Z	-1.44	-2.78	1.25	16
AU.SDAN	2018-06-10T00:00:00.000000Z	2019-12-31T23:59:59.000000Z	-1.49	-2.34	0.65	48
AU.STKA	2003-05-20T16:41:00.000000Z	2003-11-11T23:59:59.000000Z	-0.14	0.24	0.64	23
AU.STKA	2003-11-11T23:59:59.000000Z	2019-12-31T23:59:59.000000Z	30.98	30.49	0.15	899
AU.TOO	2003-06-25T00:00:00.000000Z	2019-12-31T23:59:59.000000Z	-1.2	-1.76	0.15	658
AU.WRKA	2009-04-26T00:00:00.000000Z	2019-12-31T23:59:59.000000Z	-3.23	-3.33	0.19	542
AU.XMIS	2005-08-16T00:00:00.000000Z	2019-12-31T23:59:59.000000Z	-3.36	-3.63	0.45	166
AU.YAPP	2018-06-27T23:00:32.875000Z	2019-12-31T23:59:59.000000Z	-13	-13.14	0.45	55
AU.YNG	2004-04-16T00:00:00.000000Z	2017-02-23T02:00:00.000000Z	8.73	8.42	0.31	429
AU.YNG	2017-02-23T02:00:00.000000Z	2019-12-31T23:59:59.000000Z	56	48.51	1.21	42
G.CAN	1987-11-27T00:00:00.000000Z	2019-12-31T23:59:59.000000Z	0.58	0.12	0.12	1450
II.TAU	1994-01-17T00:00:00.000000Z	2019-12-31T23:59:59.000000Z	-0.5	-0.45	0.11	1004
II.WRAB	1994-03-27T00:00:00.000000Z	2019-12-31T23:59:59.000000Z	-1.98	-1.38	0.19	954
IU.CTAO	1991-06-17T00:00:00.000000Z	2019-12-31T23:59:59.000000Z	-1.07	-0.72	0.14	1477
IU.HNR	2004-10-01T00:00:00.000000Z	2019-12-31T23:59:59.000000Z	11.24	10.48	0.84	248
IU.MBWA	2001-08-25T00:00:00.000000Z	2019-12-31T23:59:59.000000Z	0.62	0.38	0.14	1051
IU.NWAO	1991-11-25T00:00:00.000000Z	2001-09-13T04:50:00.000000Z	5.82	5.92	0.19	365
IU.NWAO	2001-09-13T04:50:00.000000Z	2019-12-31T23:59:59.000000Z	-0.59	-0.59	0.14	820
IU.PMG	1993-09-10T00:00:00.000000Z	2019-12-31T23:59:59.000000Z	0.09	1.92	1.15	31

28 Table S2: Same as Table S1, but for the *S1* network stations.

Network.Station	Start Time	End Time	Median [deg]	Mean [deg]	Std_err [deg]	N_{ev}
S1.AUALB	2013-09-26T00:00:00.000000Z	2019-12-31T23:59:59.000000Z	-1.78	-0.5	1.61	18
S1.AUALC	2015-08-19T00:00:00.000000Z	2019-12-31T23:59:59.000000Z	-6.37	-8.49	3.53	8
S1.AUAYR	2013-08-26T00:00:00.000000Z	2019-12-31T23:59:59.000000Z	-4.21	-6.04	1.4	8
S1.AUCAS	2013-08-26T00:00:00.000000Z	2019-12-31T23:59:59.000000Z	-0.9	4.41	6.81	18
S1.AUDCS	2013-05-30T00:00:00.000000Z	2019-12-31T23:59:59.000000Z	0.27	-4.12	0.87	11
S1.AUDHS	2013-08-26T00:00:00.000000Z	2019-12-31T23:59:59.000000Z	1.61	4.37	1.81	20
S1.AUHAR	2014-09-18T00:00:00.000000Z	2019-12-31T23:59:59.000000Z	-3.63	-7.9	1.2	6
S1.AUHPC	2013-05-24T00:00:00.000000Z	2019-12-31T23:59:59.000000Z	-0.31	2.35	3.09	19
S1.AUKAL	2013-09-26T00:00:00.000000Z	2019-12-31T23:59:59.000000Z	4.07	12.55	12.16	16
S1.AUKAR	2013-09-15T00:00:00.000000Z	2019-12-31T23:59:59.000000Z	3.77	1.77	3.74	5
S1.AUKSC	2013-05-24T00:00:00.000000Z	2019-12-31T23:59:59.000000Z	13.83	10.12	3.44	10
S1.AULHS	2013-10-31T00:00:00.000000Z	2019-12-31T23:59:59.000000Z	-2.56	-6.74	2.39	10
S1.AUMTS	2011-09-01T02:22:00.000000Z	2019-12-31T23:59:59.000000Z	-2.3	-3.65	0.56	26

29

30 Table S3: Same as Table S1, but for temporary stations.

Network.Station	Start Time	End Time	Median [deg]	Mean [deg]	Std_err [deg]	N_{ev}
1E.SQA01	2013-11-17T00:58:59.000000Z	2014-11-10T15:22:20.620000Z	3.5	-0.04	2.37	7
1E.SQA06	2013-11-13T03:48:59.000000Z	2014-10-14T05:20:27.020000Z	1.12	1.34	1.93	6
1E.SQA09	2013-11-14T04:42:59.000000Z	2014-11-02T17:29:06.360000Z	15.64	14.97	1.36	7
1E.SQA11	2013-11-14T00:26:59.000000Z	2014-11-06T09:31:39.640000Z	9.19	10.26	1.34	7
1K.FA10	2013-11-06T08:51:59.000000Z	2015-09-05T10:26:37.380000Z	0.05	-1.1	0.68	38
1K.FA15	2013-11-16T23:06:59.000000Z	2015-09-05T16:55:18.660000Z	-13	-12.07	0.54	18
1K.FA22	2013-11-08T06:57:59.000000Z	2014-09-03T11:07:39.340000Z	-2.02	-1.61	1.18	15
1K.FA27	2013-11-15T07:08:59.000000Z	2015-09-08T01:45:32.060000Z	-3.62	-3.88	0.71	30
1K.FA30	2013-11-07T07:40:59.000000Z	2014-09-25T00:36:32.020000Z	-9.47	-10.57	1.09	9
1K.FA36	2013-11-16T03:26:59.000000Z	2014-10-09T00:40:00.140000Z	-11.31	-10.26	0.79	13
1K.FB01	2013-11-12T04:16:59.000000Z	2015-09-09T12:11:27.900000Z	-13.05	-14.37	0.87	24
1K.FB02	2014-02-23T03:35:59.000000Z	2015-08-13T00:23:36.400000Z	-7.5	-7.87	0.59	20
1K.FB03	2013-11-13T08:30:59.000000Z	2015-09-05T03:15:22.140000Z	-8.29	-8.6	0.78	24
1K.FB04	2013-11-10T07:59:59.020000Z	2015-09-10T07:36:17.140000Z	-2.18	-2.36	0.73	24
1K.FB05	2013-11-12T06:46:59.000000Z	2015-04-23T15:33:44.620000Z	-4.86	-1.18	1.6	11
1K.FB07	2014-02-23T08:05:59.000000Z	2015-09-13T13:42:50.660000Z	-11.54	-10.77	0.67	33
1K.FB08	2014-02-23T02:39:59.000000Z	2015-08-31T00:54:58.720000Z	-9.11	-9.41	0.6	34
1K.FC42	2014-10-14T05:09:59.000000Z	2015-08-15T15:13:01.200000Z	-0.74	-1.58	0.87	11
1K.FD54	2014-10-16T04:53:59.000000Z	2015-08-22T10:36:17.020000Z	4.95	4.49	1.28	8
1K.FD56	2014-10-15T07:15:59.000000Z	2015-09-01T15:59:05.800000Z	-4.34	-4.64	0.92	13
1P.BA05	2011-06-02T21:40:59.000000Z	2012-05-13T05:08:45.140000Z	21.05	19.98	0.67	11
1P.BA06	2011-07-08T02:21:59.000000Z	2012-07-11T05:12:47.060000Z	-2.78	-15.38	0.88	6
1P.BA08	2011-06-09T03:44:59.000000Z	2012-09-04T01:17:49.460000Z	-3.55	-3.82	1.03	13
1P.BA09	2011-06-11T04:59:59.000000Z	2012-09-01T05:27:54.260000Z	-4.34	-6.12	1.73	8
1P.BA10	2011-06-17T23:40:57.000000Z	2012-08-06T05:56:48.020000Z	-0.24	1.09	0.7	14
1P.BA11	2012-01-18T03:38:59.000000Z	2012-08-06T03:00:41.300000Z	3.22	2.7	1.13	10
1P.BA12	2011-06-15T06:30:43.000000Z	2013-04-22T03:44:00.980000Z	-36.34	-24.97	0.88	9
1P.BA13	2011-06-16T01:44:59.000000Z	2013-04-22T23:04:00.980000Z	-1.8	-2	0.81	26

1P.BA14	2011-06-16T05:42:59.000000Z	2013-04-23T01:38:00.980000Z	-0.72	-2.47	0.59	23
1P.BA19	2011-06-18T02:15:19.000000Z	2013-04-24T23:08:00.980000Z	-2.68	-3.12	0.75	16
1P.BA20	2011-06-20T02:37:59.000000Z	2013-04-26T02:12:00.980000Z	4.62	3.53	0.43	21
1P.BA22	2011-06-21T01:46:59.000000Z	2013-04-28T01:21:00.980000Z	-1.63	-0.81	0.68	16
6F.BL01	2008-09-14T00:20:59.000000Z	2010-12-20T11:28:00.980000Z	4.35	5.45	0.82	17
6F.BL02	2008-09-13T06:13:59.000000Z	2011-02-20T00:00:00.980000Z	3.2	-0.95	0.74	13
6F.BL03	2008-09-13T01:15:10.000000Z	2011-02-15T07:55:00.960000Z	3.88	4.13	0.35	62
6F.BL04	2008-09-12T05:21:59.000000Z	2010-02-28T10:56:00.980000Z	5.86	7.49	0.73	22
6F.BL05	2008-09-12T00:51:59.000000Z	2009-09-12T23:36:00.980000Z	0.95	0.25	0.4	38
6F.BL06	2008-09-11T01:38:17.000000Z	2011-03-22T02:06:00.980000Z	-1.36	-2.27	0.43	91
6F.BL07	2008-09-11T07:01:02.000000Z	2011-05-16T02:17:00.980000Z	0.64	0.86	0.66	43
6F.BL08	2008-09-10T05:26:59.000000Z	2011-02-15T12:15:00.980000Z	5.86	5.34	0.61	49
6F.BL09	2008-09-10T00:49:26.000000Z	2011-05-16T04:41:00.980000Z	-1.36	-2.72	0.29	88
6F.BL10	2008-09-09T07:10:59.000000Z	2011-05-16T02:07:00.980000Z	1.08	0.42	0.34	82
6F.BL11	2008-09-09T01:26:15.000000Z	2011-05-17T00:51:00.980000Z	0.4	0.06	0.36	125
6F.BL12	2008-09-08T07:58:15.000000Z	2011-05-17T04:40:00.980000Z	2.92	2.42	0.51	59
6F.BL13	2008-09-08T01:33:20.000000Z	2011-05-19T04:35:54.980000Z	1.9	0.4	0.6	76
6F.BL14	2008-09-03T01:11:59.000000Z	2011-05-18T02:45:00.980000Z	-0.69	-1.27	0.67	46
6F.BL15	2008-09-02T09:23:59.000000Z	2011-05-18T07:40:00.980000Z	3.05	2.97	0.8	24
6F.BL16	2008-09-02T01:04:59.000000Z	2011-03-31T04:13:00.980000Z	-1.27	3.29	0.75	26
6F.BL17	2008-09-01T03:51:59.000000Z	2011-05-21T01:03:00.980000Z	1.26	2.3	0.4	62
6F.BL18	2008-08-31T08:40:54.000000Z	2010-11-11T02:04:00.980000Z	-0.26	-2.15	0.48	63
6F.BL19	2008-09-01T00:16:59.000000Z	2011-05-22T00:57:00.980000Z	2.12	0.61	0.64	44
6F.BL20	2008-08-31T01:19:59.000000Z	2010-07-12T03:40:00.980000Z	0.7	0.82	0.52	67
6F.BL23	2008-08-28T23:59:59.000000Z	2010-10-12T00:10:01.980000Z	1.5	9.37	0.27	32
6F.BL24	2008-08-28T02:18:13.000000Z	2011-05-24T00:35:00.980000Z	1.27	0.84	0.45	75
6F.BL25	2008-08-27T03:27:11.000000Z	2011-05-09T03:00:00.980000Z	1.99	1.67	0.77	14
7B.SA03	1993-05-13T01:16:11.857000Z	1993-10-05T03:22:29.526000Z	1.96	3.32	1.22	13
7B.SA04	1993-05-14T06:26:50.846000Z	1993-10-03T22:00:59.799000Z	3.83	0.75	0.8	21
7B.SA06	1993-05-05T00:44:49.846000Z	1993-09-01T00:54:49.800000Z	-0.27	0.36	0.68	10
7B.SA08	1993-05-03T03:00:57.846000Z	1993-10-10T01:30:52.798000Z	1.67	0.94	0.77	6
7B.SC01	1994-05-26T05:45:36.846000Z	1994-10-05T20:48:47.574000Z	1.52	3.93	1.1	18

7B.SC03	1994-08-05T09:40:54.846000Z	1994-10-15T19:20:56.806000Z	-5.74	-5.1	1.63	8
7B.SC05	1994-05-23T05:59:16.381000Z	1994-09-14T06:04:33.250000Z	-1.72	-0.45	1.97	10
7B.SC06	1994-06-01T00:14:07.846000Z	1994-10-17T03:27:48.800000Z	-3.74	-3.78	1.56	10
7B.SC10	1994-08-09T03:59:03.846000Z	1994-10-19T13:59:05.639000Z	2.32	7.54	1.95	6
7B.SD02	1995-03-20T06:17:29.846000Z	1995-05-07T06:37:31.806000Z	3.04	3.4	0.96	10
7B.SD03	1995-03-23T06:11:46.846000Z	1995-08-07T03:08:31.516000Z	2.86	3.37	0.68	14
7B.SD05	1995-03-19T04:34:22.846000Z	1995-08-04T14:27:15.963000Z	1.24	1.5	1.13	8
7B.SD06	1995-03-18T02:38:46.846000Z	1995-05-24T02:28:48.098000Z	5.14	3.92	0.92	12
7B.SD07	1995-03-26T07:49:26.846000Z	1995-07-08T00:00:00.976000Z	-2.88	-3.87	2.5	6
7B.SD08	1995-03-27T09:03:21.842000Z	1995-08-10T01:25:17.015000Z	-0.31	-0.07	1.34	12
7B.SD10	1995-03-31T07:38:35.846000Z	1995-06-03T06:48:39.346000Z	0.34	0.66	0.92	8
7D.KA02	1997-07-21T03:17:09.846000Z	1997-10-07T08:47:12.016000Z	3.33	3.78	1.32	8
7D.KA09	1997-07-27T04:26:09.846000Z	1997-10-13T02:07:21.806000Z	7.98	6.51	1.83	10
7F.QA01	1999-03-04T01:17:40.720000Z	1999-06-29T03:28:32.920000Z	8.7	8.79	2.32	5
7F.QR01	1999-05-14T13:54:18.760000Z	1999-11-04T05:19:10.800000Z	4.85	-2.63	0.5	10
7F.QR07	1999-03-24T07:38:11.840000Z	1999-10-28T05:37:15.600000Z	-8.69	-8.79	1.27	7
7F.QR08	1999-03-22T04:06:11.840000Z	1999-10-04T05:06:19.480000Z	-13.36	-13.39	1.53	8
7F.QR09	1999-03-22T23:54:37.840000Z	1999-06-12T03:26:16.040000Z	-13.19	-13.47	0.76	6
7F.QR10	1999-03-24T00:54:45.400000Z	1999-10-27T10:25:02.520000Z	-17.63	-16.92	1.46	8
7G.WR02	2000-07-15T04:17:48.720000Z	2001-01-29T07:33:21.815300Z	2.24	2.04	0.9	12
7G.WR04	2000-07-20T04:04:12.712300Z	2001-01-28T03:34:21.465200Z	2.49	3.09	1.36	14
7G.WR05	2000-07-19T02:25:43.720000Z	2001-07-13T02:32:14.820100Z	-3.36	-2.33	0.74	27
7G.WR06	2000-07-11T04:19:57.720000Z	2001-01-31T07:49:11.102700Z	-8.36	-8.05	0.67	30
7G.WR07	2000-07-21T06:29:08.720000Z	2000-10-13T02:01:40.299400Z	-2.23	-1.24	1.33	10
7G.WR08	2000-10-21T06:32:29.719900Z	2001-07-05T03:07:43.343900Z	-1.6	-1.03	0.81	21
7G.WR09	2000-10-12T02:53:58.720000Z	2001-07-06T04:57:10.175800Z	6.39	4.86	1.17	24
7H.TA01	2001-10-04T03:19:27.840000Z	2002-07-18T21:22:44.200000Z	6.49	6.93	0.43	6
7H.TA04	2001-10-05T01:46:50.720000Z	2002-07-03T00:37:34.720000Z	-1.45	0.4	0.85	10
7H.TA06	2001-10-06T01:14:39.720000Z	2002-08-07T01:04:29.440000Z	-1.29	-3.63	0.61	7
7H.TA10	2001-10-11T00:36:33.720000Z	2002-08-16T00:54:24.520000Z	-3.13	0.72	0.64	11
7H.TA11	2001-10-08T04:35:41.720000Z	2002-08-15T01:58:40.040000Z	4.13	5.37	0.38	10
7H.TA12	2001-10-07T23:30:51.720000Z	2002-08-15T00:18:47.280000Z	0.31	-4.39	1.51	8

7H.TB03	2001-12-13T00:03:48.840000Z	2002-05-15T08:12:10.560000Z	-3.27	-2.53	1.02	8
7I.GA06	2004-06-05T01:25:40.520000Z	2004-12-31T23:57:33.800000Z	-6.3	-4.36	0.94	9
7I.GA07	2004-06-05T06:09:39.840000Z	2005-04-14T00:48:40.800000Z	-0.91	-1.66	1.64	8
7I.GA08	2004-11-19T02:02:38.880000Z	2005-04-14T23:33:46.440000Z	-3.41	-4.69	0.87	10
7I.TL01	2003-05-28T04:37:01.680000Z	2005-05-23T11:37:32.240000Z	-0.19	0.21	0.57	29
7I.TL02	2003-05-29T03:00:28.680000Z	2005-06-02T03:48:31.640000Z	-1.33	0.25	0.51	31
7I.TL03	2003-05-26T05:31:03.680000Z	2004-09-27T04:30:17.800000Z	-4.14	-4.58	0.85	13
7I.TL04	2003-05-27T03:51:59.000000Z	2004-01-01T00:00:00.960000Z	1.44	-0.08	0.96	15
7I.TL05	2003-05-30T02:28:59.000000Z	2005-06-04T01:28:54.720000Z	-3.84	-3.85	1.09	6
7I.TL06	2003-05-25T07:28:59.000000Z	2004-11-13T03:44:22.080000Z	-0.67	-0.9	0.38	57
7I.TL07	2003-05-25T02:21:59.000000Z	2005-03-14T08:00:00.960000Z	1.26	2.96	0.52	41
7I.TL08	2003-06-01T02:59:59.000000Z	2005-06-04T02:09:25.440000Z	0.47	-0.53	0.78	16
7I.TL09	2003-05-23T03:19:59.000000Z	2005-05-27T03:25:33.120000Z	-0.95	10.82	1.42	8
7I.TL10	2003-06-02T01:09:34.720000Z	2005-06-05T00:00:39.080000Z	-6.1	-4.76	0.76	19
7I.TL12	2003-05-22T07:16:59.000000Z	2005-11-17T05:02:42.240000Z	-2.25	1.43	1.42	23
7I.TL14	2003-05-02T02:59:59.000000Z	2005-08-18T00:00:00.960000Z	-4.37	-4.05	0.72	38
7I.TL15	2003-05-21T00:27:59.000000Z	2005-08-18T00:00:00.960000Z	-3.83	-3.46	0.59	26
7I.TL16	2003-05-01T00:29:59.000000Z	2005-04-19T03:09:25.440000Z	2.4	0.86	0.94	18
7I.TL17	2003-05-03T03:27:59.000000Z	2005-08-18T00:00:00.960000Z	-1.42	-1.07	0.4	30
7I.TL18	2003-05-04T01:25:00.840000Z	2005-08-17T23:00:00:00.960000Z	-7.62	-7.39	0.75	43
7I.TL19	2003-12-02T03:45:59.000000Z	2004-11-16T03:02:42.240000Z	1.68	2.36	2.43	7
7J.CP01	2006-06-18T08:23:52.000000Z	2007-05-25T00:00:00.960000Z	1.28	1.04	0.51	40
7J.CP02	2006-06-18T04:36:59.000000Z	2007-04-05T02:00:00.960000Z	3.91	1.96	0.42	21
7J.CP03	2006-06-21T07:49:29.000000Z	2007-05-28T00:00:00.960000Z	1.84	0.68	0.77	17
7J.CP04	2006-06-22T01:38:46.000000Z	2006-11-24T06:57:00.960000Z	4.85	4.74	1.06	20
7J.CP05	2006-06-22T06:26:59.000000Z	2007-05-29T00:00:00.960000Z	8.3	7.67	0.56	30
7J.CP06	2006-06-23T07:14:28.000000Z	2007-05-29T00:00:00.960000Z	-2.26	-2.19	1.07	22
7J.CP08	2006-11-14T23:59:59.000000Z	2007-05-30T06:27:00.960000Z	-1.18	-2.81	0.63	20
7J.CP09	2006-06-25T07:01:59.000000Z	2007-05-31T00:00:00.960000Z	1	-0.31	0.96	15
7J.CP10	2006-06-25T02:51:59.000000Z	2007-05-31T00:00:00.960000Z	-1.13	0.54	0.71	25
7J.CP11	2006-06-26T03:59:59.000000Z	2007-01-06T00:00:00.960000Z	1.21	-0.93	0.77	20
7J.CP12	2006-06-26T06:36:20.000000Z	2007-01-06T00:00:00.960000Z	-4.93	-4.04	0.74	19

7J.CP13	2006-11-17T23:59:59.000000Z	2007-02-06T00:00:00.960000Z	-2.02	-2.04	1.11	11
7J.CP14	2006-06-27T07:33:59.000000Z	2007-02-06T00:00:00.960000Z	1.24	1.44	0.52	34
7J.LP02	2005-10-20T02:44:30.846000Z	2007-01-11T12:21:47.844000Z	-2.88	-3.25	0.99	12
7J.LP05	2006-02-04T07:22:13.846000Z	2007-02-05T00:00:00.966000Z	4.17	2.63	1.53	14
7J.RP01	2006-02-04T03:12:14.846000Z	2007-01-05T00:00:00.966000Z	-6.84	-5.71	0.78	13
7J.RP03	2006-06-19T03:26:17.000000Z	2007-05-27T00:00:00.960000Z	0.91	-2.75	0.71	15
7J.RP04	2006-06-21T01:28:59.000000Z	2007-05-27T00:00:00.960000Z	1.64	6.19	0.69	18
7J.RP06	2006-06-20T07:46:59.000000Z	2007-05-26T00:00:00.960000Z	2.38	2.35	1.73	10
7K.MUR03	2007-02-19T01:06:05.718100Z	2008-04-29T18:05:59.998500Z	-8.29	-7.82	1.6	7
7K.MUR04	2007-02-20T00:40:11.718000Z	2008-03-07T00:00:01.935400Z	-3.91	-1.98	0.92	9
7K.MUR05	2007-02-21T06:35:16.718000Z	2008-02-06T00:00:01.669100Z	2.4	0.16	0.75	10
7K.SOC03	2007-07-25T06:57:39.720000Z	2008-06-16T23:18:17.921200Z	2.71	2.5	1.26	6
7K.SOC04	2008-01-21T22:48:59.000000Z	2008-06-16T00:00:00.960000Z	4.9	5.28	1.25	13
7K.SOC05	2007-09-07T23:59:59.000000Z	2008-06-18T23:55:47.520000Z	1.92	1.14	1.15	7
7K.SOC06	2007-08-06T03:05:59.000000Z	2008-06-19T05:22:51.840000Z	-2.57	-2	0.85	28
7K.SOC07	2007-10-24T02:08:59.000000Z	2008-08-14T03:53:46.560000Z	0.15	-0.2	0.5	19
7K.SOC08	2007-10-25T03:27:59.000000Z	2008-08-13T00:00:00.960000Z	1.97	0.5	0.46	33
7K.SOC09	2007-10-27T03:02:59.000000Z	2008-08-12T01:22:51.840000Z	-0.08	-0.36	1.32	12
7K.SOC11	2007-10-28T23:59:59.000000Z	2008-08-10T00:50:24.960000Z	-2.53	-8.75	1.54	9
7K.SOC12	2007-10-29T02:46:59.000000Z	2008-08-09T02:02:42.240000Z	3.85	3.43	0.9	15
7K.SOC13	2007-10-30T03:37:53.000000Z	2008-08-08T00:00:00.960000Z	0.96	1.96	0.65	29
7K.SOC14	2007-10-31T02:28:59.000000Z	2008-07-09T00:00:00.960000Z	0.74	1.91	1.58	8
7K.SOC15	2007-11-01T23:59:59.000000Z	2008-06-09T00:00:00.960000Z	-1.54	-3.13	0.7	36
7K.SOC16	2007-11-01T08:01:59.000000Z	2008-06-08T00:00:00.960000Z	2.62	2.4	0.92	22
YS.ALRB	2014-11-11T07:26:54.380000Z	2018-12-31T23:59:59.000000Z	-2.35	-1.49	0.53	41
YS.BAOP	2014-11-01T00:00:00.000000Z	2016-10-10T07:26:09.200000Z	-14.02	-14.08	0.53	42
YS.BKOR	2014-10-28T04:59:59.200000Z	2016-11-05T02:13:03.180001Z	-1.66	-8.03	0.53	55
YS.ENDE	2014-11-03T05:33:32.200000Z	2018-12-31T23:59:59.000000Z	-6.36	-6.91	0.52	42
YS.HADA	2014-11-01T04:13:50.200000Z	2016-10-11T00:05:59.180001Z	-3.8	-3.7	0.4	105
YS.LMBR	2014-11-06T07:41:25.200000Z	2016-11-08T02:36:46.180001Z	-3.37	8.93	0.83	10
YS.SINA	2014-10-29T07:03:10.200000Z	2016-11-05T06:47:01.180001Z	3.18	4.92	1.01	39